Low-Dimensional Reduced-Order Models for Statistical Response and Uncertainty Quantification: Two-layer Baroclinic Turbulence

Di Qi* and Andrew J. Majda

Department of Mathematics and Center for Atmosphere and Ocean Science, Courant Institute of Mathematical Sciences, New York University, New York, NY 10012

**Corresponding author address:* Department of Mathematics and Center for Atmosphere and Ocean Science, Courant Institute of Mathematical Sciences, New York University, New York, NY 10012.

E-mail: qidi@cims.nyu.edu (Di Qi), jonjon@cims.nyu.edu (Andrew Majda)

Generated using v4.3.2 of the AMS LaTeX template

ABSTRACT

Accurate uncertainty quantification for the mean and variance about forced responses to general external perturbations in the climate system is an important subject in understanding the earth's atmosphere and ocean in climate change science. Here a low-dimensional reduced-order method is developed for uncertainty quantification and capturing the statistical sensitivity in principal model directions with largest variability, and in various regimes in two-layer quasi-geostrophic turbulence. Typical dynamical regimes tested here include the homogeneous flow in high-latitude and the anisotropic meandering jets in low/mid-latitude. The idea in the reduced-order method is from a self-consistent mathematical framework for general systems with quadratic nonlinearity, where crucial high-order statistics are approximated by a systematic model calibration procedure. Model efficiency is improved through additional damping and noise corrections to replace the expensive energy-conserving nonlinear interactions. Model errors due to the imperfect nonlinear approximation are corrected by tuning the model parameters using linear response theory with an information metric in a training phase before prediction. Here a statistical energy principle is adopted to introduce a global scaling factor in characterizing the higher-order moments in a consistent way to improve model sensitivity. The reduced-order model displays uniformly high prediction skill for the mean and variance response to general forcing for both homogeneous flow and anisotropic zonal jets in the first 10^2 dominant low-wavenumber modes, where only about 0.15% of the total spectral modes are resolved, compared with the full model resolution of 256^2 horizontal modes.

1. Introduction

The climate system is a complex chaotic multi-scale system combining forcing, dissipation, and nonlinear energy-conserving interactions displaying significant complexity. Accurate modeling of the large-scale variability in the earth's atmosphere and ocean to changes in external forcing is a central problem of contemporary climate change science (Zurita-Gotor et al. 2014; Gettelman et al. 2012; Majda and Wang 2006; Deser and Blackmon 1993; Treguier and Hua 1987). Nonlinear turbulent interactions may be important or dominant in maintaining the general circulation in atmosphere and ocean, so accurate characterization of the higher-order effects becomes crucial. There is a need to understand the evolution of fluctuations in the atmosphere/ocean circulation where various kinds of instabilities frequently take place.

One simple but fully nonlinear fluid model which is particularly relevant to meteorology and oceanography is the two-layer quasi-geostrophic (QG) model with baroclinic instability in a two-dimensional periodic domain (Vallis 2006; Salmon 1998). It is known that the QG model is quite capable in capturing the essential physics of the relevant internal variability despite its relatively simple dynamical structure (Vallis 2006; Salmon 1998). The flow is usually driven at low wavenumbers and damped by boundary friction. Two dynamical regimes in the QG model with typical statistical features are representative in many applications (Treguier and Hua 1987; Panetta 1993; Thompson and Young 2007; Grooms and Majda 2013). The first one is the fully turbulent flow with homogeneous statistics as a result of internal baroclinic instability corresponding to the high-latitude ocean and atmosphere; the second one is the anisotropic flow field with strong meandering zonal jets as in the low/mid-latitude regime.

The quasi-geostrophic response to both stochastic and deterministic perturbations is an important subject in understanding the earth's atmospheric and oceanic interactions (Abramov and Majda 2012; Deser and Blackmon 1993; Lutsko et al. 2015). The external perturbations can be induced by various forcing mechanisms. In the ocean regime, one important category of perturbation can be introduced from *the atmospheric forcing effects* that drive the oceanic circulation. For example, the large-scale, long-time sea surface temperature (SST) anomalies can be explained naturally as the response of the oceanic surface layers to short-time-scale atmospheric forcing (Kushnir 1994; Deser and Blackmon 1993). The atmospheric forcing can be caused by *wind stress, radiative heating, pressure fluctuations, or buoyancy fluxes at the surface*. It is therefore important to investigate the nature of the atmospheric and oceanic variability induced by the various external effects, especially from the fluctuating component.

Linear response theory together with the fluctuation-dissipation theorem (FDT) provides a method for calculating responses to small external perturbations through the knowledge of the unperturbed statistical system with many practical applications (Leith 1975; Majda et al. 2005; Majda and Wang 2010; Gritsun and Branstator 2007; Gritsun et al. 2008). Several studies have tested the idea of using FDT, in the form introduced to climate science first in Leith (1975), to generate a linear operator that approximates the response of a general circulation model to any specified weak external source. The FDT approach has been applied for complex climate models with various approximations and numerical procedures. A quasi-Gaussian approximation has been applied to many problems (Abramov and Majda 2012; Lutsko et al. 2015; Gritsun et al. 2008) and a more practical low-frequency approach in a subspace has been developed in Majda et al. (2010). However this method is hampered by the fundamental limitation to parameter regimes with linear statistical response. Thus new strategies for imperfect low-order models on subspace that capture both the mean and variance response, *i.e.* quantify uncertainty, are important and a main theme of present research (Sapsis and Majda 2013a,b; Majda and Qi 2016; Qi and Majda 2016). The low-order models focus on the variability in the principal directions of the system which are most energetic, and approximate the higher-order nonlinear interactions through proper closure strategies using only lower-order statistics (Qi and Majda 2016). Thus the accurate calibration about the statistical energy transfer in third-order moments plays a crucial role in the closure model construction.

Our goal in this paper is to develop efficient reduced-order statistical models based on a detailed study about the role of high-order statistical symmetry in transferring the energy from the production wavenumbers (large-scales) to the dissipation wavenumbers (small-scales). The basic idea of this statistical reduced-order method is introduced in Majda and Qi (2016) and the feasibility has been tested successfully on simpler models such as the 40-dimensional Lorenz-96 system and the barotropic system with topography (Majda and Qi 2016; Qi and Majda 2016). The expensive higher-order moments in the true statistical dynamics are replaced by efficient additional nonlinear damping and noise corrections using only first and second order moment information. The imperfect model error through this approximation is calibrated through an information-theoretic framework using relative entropy (Majda and Gershgorin 2011; Majda et al. 2005). A systematic framework is proposed to improve model prediction skill and achieve the optimal model parameter for various kinds of external perturbations in a training phase using only statistics from unperturbed equilibrium statistics. In the training phase, linear response theory is used to calculate the kicked linear response operator that characterizes the model sensitivity to perturbations. The model sensitivity to different external perturbation forcings is further improved using the total statistical energy as a global scaling factor through a simple scalar dynamical equation developed in Majda (2015, 2016).

The performance of the reduced-order method is then tested on various dynamical regimes of the two-layer QG equations with distinct statistical features. Specifically we consider the high-latitude atmosphere and ocean regime with homogeneous statistics, and the low/mid-latitude regime where anisotropic zonal jets are developed in both the atmosphere and ocean. These are two representative dynamical regimes with direct relevance to realistic atmosphere and ocean flows. The influence of nonlinear energy transfer due to the forcing perturbation cannot be neglected in these parameter ranges where nonlinearities are important. The unified systematic procedure is applied for portable low-dimensional reduced-order computational models that possess the skill in capturing the sensitivity in principal directions with largest variability, while effectively reduce the computational cost at the same time. The reduced-order models display uniformly high prediction skill in all these dynamical regimes by only calculating the first 10×10 dominant modes, where only about 0.15% of the total spectral modes are resolved, compared with the full model resolution of 256×256 modes.

The structure of the paper is arranged as follows. Section 2 describes the basic statistical formulation and the important statistical formulas for the total statistical energy is derived for the two-layer flow. The low-dimensional reduced-order model is developed in Section 3 with detailed discussions about the calibration strategy according to the symmetry in the higher-order moments. The feasibility of the reduced-order model is tested in different dynamical regimes in the following parts. Section 4 shows the results in high-latitude regime with homogenous statistics, and Section 5 considers the low/mid-latitude regime where anisotropic jets introduce distinct structure in the the flow fields. Finally, Section 6 contains a summary of the results as well as an outlook on future developments.

2. Two-layer quasi-geostrophic turbulence and the statistical theories

a. Two-layer barotropic-baroclinic flow with forcing and dissipation

We consider a fluid system in the rotational reference frame comprised of two layers of equal depth between rigid lid and flat bottom. The governing two-layer quasi-geostrophic (QG) equations in a barotropic-baroclinic mode formulation for potential vorticity anomalies $\left(q_\psi, q_\tau\right)$ with periodic boundary condition in both x, y directions are (Salmon 1998; Vallis 2006)

$$
\begin{aligned}
\frac{\partial q_\psi}{\partial t}+J\left(\psi, q_\psi\right)+J\left(\tau, q_\tau\right)+\beta\frac{\partial \psi}{\partial x}+U\frac{\partial}{\partial x}\Delta\tau &= -\frac{\kappa}{2}\Delta\left(\psi-\tau\right)-\nu(-1)^s\Delta^s q_\psi+\mathscr{F}_\psi\left(\mathbf{x},t\right),\\
\frac{\partial q_\tau}{\partial t}+J\left(\psi, q_\tau\right)+J\left(\tau, q_\psi\right)+\beta\frac{\partial \tau}{\partial x}+U\frac{\partial}{\partial x}\left(\Delta\psi+k_d^2\psi\right) &= \frac{\kappa}{2}\Delta\left(\psi-\tau\right)-\nu(-1)^s\Delta^s q_\tau+\mathscr{F}_\tau\left(\mathbf{x},t\right).
\end{aligned}
\tag{1}
$$

Above $q_\psi=\Delta\psi$, $q_\tau=\Delta\tau-k_d^2\tau$ are the *disturbance* potential vorticity in the barotropic and baroclinic modes respectively, while ψ, τ are the corresponding *disturbance* barotropic and baroclinic stream functions. The barotropic mode ψ can be viewed as the vertically averaged effect from the flow, and the baroclinic mode τ is usually related with the thermal effect in heat transport. The relations between the upper and lower layer variables and the barotropic and baroclinic mode can be defined through the following relations

$$
\begin{aligned}
q_\psi=\nabla^2\psi=\frac{1}{2}\left(q_1+q_2\right),\ \psi=\frac{1}{2}\left(\psi_1+\psi_2\right),\\
q_\tau=\nabla^2\tau-k_d^2\tau=\frac{1}{2}\left(q_1-q_2\right),\ \tau=\frac{1}{2}\left(\psi_1-\psi_2\right).
\end{aligned}
$$

Besides, $J\left(A,B\right)=A_xB_y-A_yB_x$ represents the Jacobian operator. $k_d=\sqrt{8}/L_d=\left(2f_0/NH\right)^2$ is the baroclinic deformation wavenumber corresponding to the Rossby radius of deformation L_d. A large-scale vertical shear $\left(U,-U\right)$ with the same strength and opposite directions is assumed in the background to induce baroclinic instability. In the dissipation operators on the right hand sides of the equations (1), besides the hyperviscosity, $\nu\Delta^s q_i$, we only use Ekman friction, $\kappa\Delta\psi_2$, with strength κ on the lower layer of the flow.

The forcing terms on barotropic and baroclinic modes, $\mathscr{F}_\psi, \mathscr{F}_\tau$, are decomposed into the deterministic part, and the random component represented by Gaussian white noises

$$\begin{aligned}\mathscr{F}_\psi(\mathbf{x},t) &= f_\psi(\mathbf{x},t) + \sigma_\psi(\mathbf{x})\dot{W}_\psi(t),\\ \mathscr{F}_\tau(\mathbf{x},t) &= f_\tau(\mathbf{x},t) + \sigma_\tau(\mathbf{x})\dot{W}_\tau(t).\end{aligned} \tag{2}$$

Examples of the large-scale forcing terms can include radiative heating, surface wind stress etc., while wind stress, convective storms, unresolved baroclinic instability process can act as the forcing on small length scales (Majda and Wang 2006; Vallis 2006). Usually the two-layer system will reach an equilibrium statistical steady state without any forcing perturbations, and we will mostly focus on investigating the system's deviation from the unperturbed equilibrium state due to various external effects from nature.

b. Formulation of the exact statistical moment dynamics

Normalized equations and symmetries in the nonlinear quadratic forms

We formulate the two-layer QG system with Galerkin truncation to finite number of spectral modes. Consider the truncated spectral expansion of the barotropic and baroclinic mode, (ψ_N, τ_N), with a high wavenumber truncation N under standard Fourier basis $\mathbf{e_k} = \exp(i\mathbf{k}\cdot\mathbf{x})$ due to the periodic boundary condition

$$\psi_N = \sum_{1\leq|\mathbf{k}|\leq N} \psi_{\mathbf{k}} e^{i\mathbf{k}\cdot\mathbf{x}}, \ \tau_N = \sum_{1\leq|\mathbf{k}|\leq N} \tau_{\mathbf{k}} e^{i\mathbf{k}\cdot\mathbf{x}}.$$

In model simulations, it is useful to introduce a new set of rescaled normalized quantities so that

$$\begin{aligned}p_{\psi,\mathbf{k}} &= q_{\psi,\mathbf{k}}/|\mathbf{k}| = -|\mathbf{k}|\,\psi_{\mathbf{k}},\\ p_{\tau,\mathbf{k}} &= q_{\tau,\mathbf{k}}/\sqrt{|\mathbf{k}|^2+k_d^2} = -\sqrt{|\mathbf{k}|^2+k_d^2}\,\tau_{\mathbf{k}}.\end{aligned} \tag{3}$$

The introduction of this new set of quantities (3) offers convenience that the energy inner-product becomes the standard Euclidean form, and p_ψ, p_τ can share the similar order of amplitude especially for the ocean case with larger k_d. Under the above set-up, the rescaled set of equations of (1) can be summarized in the form for each wavenumber as

$$\frac{d\mathbf{p_k}}{dt} = B_\mathbf{k}\left(\mathbf{p_k},\mathbf{p_k}\right) + \left(\mathscr{L}_\mathbf{k} - \mathscr{D}_\mathbf{k}\right)\mathbf{p_k} + \mathscr{F}_\mathbf{k}, \quad \mathbf{p_k} = \left(p_{\psi,\mathbf{k}}, p_{\tau,\mathbf{k}}\right)^T, \tag{4}$$

where the linear operators are decomposed into the non-symmetric part $\mathscr{L}_\mathbf{k}$ involving β-effect and vertical shear flow U and dissipation part $\mathscr{D}_\mathbf{k}$, together with the forcing $\mathscr{F}_\mathbf{k}$ combining deterministic component and stochastic component (see Appendix A for explicit formulas).

Most importantly, $B(\mathbf{p},\mathbf{p})$ is the nonlinear interaction so that

$$B_\mathbf{k}\left(\mathbf{p_k},\mathbf{p_k}\right) = \begin{bmatrix} B_{\psi,\mathbf{k}} \\ B_{\tau,\mathbf{k}} \end{bmatrix} = \begin{bmatrix} \sum_{\mathbf{m}+\mathbf{n}=\mathbf{k}} \frac{\mathbf{m}^\perp\cdot\mathbf{n}}{|\mathbf{k}|}\left(\frac{|\mathbf{n}|}{|\mathbf{m}|}p_{\psi,\mathbf{m}}p_{\psi,\mathbf{n}} + \sqrt{\frac{|\mathbf{n}|^2+k_d^2}{|\mathbf{m}|^2+k_d^2}}p_{\tau,\mathbf{m}}p_{\tau,\mathbf{n}}\right) \\ \sum_{\mathbf{m}+\mathbf{n}=\mathbf{k}} \frac{\mathbf{m}^\perp\cdot\mathbf{n}}{\sqrt{|\mathbf{k}|^2+k_d^2}}\left(\frac{\sqrt{|\mathbf{n}|^2+k_d^2}}{|\mathbf{m}|}p_{\psi,\mathbf{m}}p_{\tau,\mathbf{n}} + \frac{|\mathbf{n}|}{\sqrt{|\mathbf{m}|^2+k_d^2}}p_{\tau,\mathbf{m}}p_{\psi,\mathbf{n}}\right) \end{bmatrix}. \tag{5}$$

One important property of the system (4) is the symmetry in the nonlinear quadratic interaction term that conserves both energy and enstrophy (Salmon 1998; Sapsis and Majda 2013a). With the inner-product defined according to the energy or enstrophy, the nonlinear interaction always satisfies the conservation law $\sum_\mathbf{k}\mathbf{p_k}\cdot B_\mathbf{k}\left(\mathbf{p_k},\mathbf{p_k}\right) = 0$, meaning that the nonlinear interaction will not change the total energy and enstrophy inside the system. Furthermore, it can be shown that a detailed triad energy conservation symmetry (see Majda 2015, 2016) is guaranteed in the nonlinear term. Therefore, a statistical energy principle can be developed for the two-layer system (4) following the general theoretical framework (Majda 2015), with the help of which we can estimatethe total statistical energy structure.

STATISTICAL MOMENT DYNAMICS OF THE TWO-LAYER SYSTEM

Due to the turbulent nature of the system, it is more useful to investigate the dynamical evolution of the statistical moments in the state variables of interest. We consider the combined *statistical energy in each mode* including variability in both mean and variance

$$R_{\mathbf{k}}=\overline{\mathbf{p_k}^{*}\mathbf{p_k}}=\begin{bmatrix}\overline{\left|p_{\psi,\mathbf{k}}\right|^{2}} & \overline{p_{\psi,\mathbf{k}}^{*}p_{\tau,\mathbf{k}}}\\ \overline{p_{\psi,\mathbf{k}}p_{\tau,\mathbf{k}}^{*}} & \overline{\left|p_{\tau,\mathbf{k}}\right|^{2}}\end{bmatrix},\tag{6}$$

where the 'overbar' can be viewed as ensemble average combining energy in the mean and covariance, $\overline{p_{1,\mathbf{k}}^{*}p_{2,\mathbf{k}}}=\bar{p}_{1,\mathbf{k}}^{*}\bar{p}_{2,\mathbf{k}}+\overline{p_{1,\mathbf{k}}^{\prime *}p_{2,\mathbf{k}}^{\prime}}$. Note that in the homogeneous case (see Section 4 for the results in high latitudes) where the equilibrium mean and the cross-covariance between different wavenumber modes are both vanishing, $R_{\mathbf{k}}$ becomes exactly the covariance matrix between barotropic and baroclinic modes; on the other hand, when anisotropic structure is generated (like in the regime with jets in Section 5), $R_{\mathbf{k}}$ will combine variabilities in both mean and variance. The idea to use the statistical energy in each mode $R_{\mathbf{k}}$ is to construct a unified framework for predicting responses in different regimes, and at the same time avoid the possibly complicated mean-covariance interaction terms if mean and variance dynamics are considered individually.

Therefore the true dynamical equations for the statistical moment $R_{\mathbf{k}}$ in the form of a 2×2 matrix containing barotropic and baroclinic mode in the same wavenumber $\mathbf{k}$ become

$$\frac{dR_{\mathbf{k}}}{dt}=\left(\mathscr{L}_{\mathbf{k}}-\mathscr{D}_{\mathbf{k}}\right)R_{\mathbf{k}}+Q_{F,\mathbf{k}}+Q_{\sigma,\mathbf{k}}+c.c.,\quad \left|\mathbf{k}\right|\leq N,\tag{7}$$

where $c.c.$ represents the complex completion for the conjugate parts. On the right hand side of the equation, $\mathscr{L}_{\mathbf{k}},\mathscr{D}_{\mathbf{k}}$, the same as the previous equations (4), represent the linear interactions between modes, including β-effect through the rotation of the earth, the effects from the mean shear flow U, as well as the dissipations from Ekman drag and hyperviscosity. $Q_{\sigma,\mathbf{k}}$ is the external forcing perturbations represented by hypothetical stirring and heating forces. Importantly, the nonlinear flux

$$Q_{F,\mathbf{k}} = \overline{\mathbf{p_k}^* B_\mathbf{k}\left(\mathbf{p_k},\mathbf{p_k}\right)} = \begin{bmatrix} \overline{\mathbf{p}^*_{\psi,\mathbf{k}} B_{\psi,\mathbf{k}}} & \overline{\mathbf{p}^*_{\psi,\mathbf{k}} B_{\tau,\mathbf{k}}} \\ \overline{\mathbf{p}^*_{\tau,\mathbf{k}} B_{\psi,\mathbf{k}}} & \overline{\mathbf{p}^*_{\tau,\mathbf{k}} B_{\tau,\mathbf{k}}} \end{bmatrix}, \tag{8}$$

represents the nonlinear interactions between different wavenumbers due to the advection term. Third-order moments with triad modes $\mathbf{m}+\mathbf{n}=\mathbf{k}$ enter the first two order moments dynamics representing the nonlinear energy transfer between small and large scales. The nonlinear energy exchange mechanism is crucial in the energy budget and will be discussed in more detail in following sections. The conservation property is also satisfied due to the triad symmetry as $\sum_\mathbf{k} \mathrm{tr} Q_{F,\mathbf{k}} = 0$. The explicit formulations of the operators can be found in Appendix A.

c. Statistical energy conservation principle

The total statistical energy dynamical equation concerns the evolution of the total variability in mean and variance in response to external perturbations (Majda 2015, 2016). With the normalized variables introduced in (3), the total statistical energy in the two-layer system can be defined through

$$E = \frac{1}{2}\sum_{1\leq|\mathbf{k}|\leq N} |\mathbf{k}|^2 \overline{|\psi_\mathbf{k}|^2} + \left(|\mathbf{k}|^2 + k_d^2\right)\overline{|\tau_\mathbf{k}|^2} = \frac{1}{2}\sum_{1\leq|\mathbf{k}|\leq N} \overline{\left|p_{\psi,\mathbf{k}}\right|^2} + \overline{\left|p_{\tau,\mathbf{k}}\right|^2}. \tag{9}$$

The exact dynamics for the statistical energy can be derived following the general framework described in Majda (2015) as

$$\frac{dE}{dt} + H_f = -\kappa E + \frac{\kappa}{2}F - \nu H + Q_\sigma. \tag{10}$$

The nonlinear interaction terms in $B\left(\mathbf{p},\mathbf{p}\right)$ will not alter the total statistical energy structure due to the detailed triad symmetry (Majda 2015). This is consistent with the total energy conserving relation in the nonlinear flux term, $\sum_\mathbf{k} \mathrm{tr} Q_{F,\mathbf{k}} = 0$. However, due to the baroclinic instability in the two-layer model, statistical energy is no longer conserved as in the barotropic case. H_f is the meridional heat flux due to baroclinic instability

$$H_f = k_d^2 U \int \overline{\psi_x \tau} = k_d^2 U \sum i k_x \overline{\psi_{\mathbf{k}}^* \tau_{\mathbf{k}}},$$

that transfers energy from the unstable baroclinic modes to the barotropic ones. F is the additional damping effects due to the non-symmetry in Ekman drag only applied on the bottom layer, which is related with the potential energy and the cross-covariance between modes

$$F = \sum k_d^2 \overline{|\tau_{\mathbf{k}}|^2} + 2\,|\mathbf{k}|^2\,\mathfrak{Re}\,\overline{\psi_{\mathbf{k}}^* \tau_{\mathbf{k}}}.$$

And νH is the additional dissipation from the hyperviscosity. Finally Q_σ adds the stochastic external perturbations to the system as an additional energy source term. We display the explicit formulation about the statistical energy equation also in Appendix A.

3. General low-dimensional reduced-order statistical methods for principal responses

In this section, we describe the general framework of the reduced-order models that can capture the statistical responses to perturbations in the most energetic and sensitive directions. In the first place, the ideas in linear response theory are introduced which can offer an effective way to estimate the linear leading order responses and calibrate imperfect model errors in the training phase. On the other hand, as the perturbation amplitudes increase, reduced-order dynamical models offer more accurate way to capture nonlinear responses. Following the systematic information-theoretical framework introduced in Majda and Qi (2016); Qi and Majda (2016), we develop the low-dimensional reduced-order models for the two-layer baroclinic turbulence which can resolve model variability along principal directions with both accuracy and efficiency.

a. Linear statistical response theory with deterministic and stochastic perturbation

The linear response theory and fluctuation-dissipation theory (FDT) offer a convenient way to get leading-order linear approximation about model responses to perturbations (Leith 1975; Majda et al. 2005; Majda and Wang 2010; Abramov and Majda 2012). Here we consider system perturbation as a combination of deterministic and stochastic random noise

$$\delta\mathbf{F}=\delta f\left(t\right)\mathbf{a}\left(\mathbf{u}\right)+\sqrt{\delta f}\left(t\right)\boldsymbol{\sigma}\left(\mathbf{x}\right)\dot{\mathbf{W}}. \tag{11}$$

We assume zero forcing, $\mathbf{F}\equiv\mathbf{0},\sigma_0\equiv 0$, in the unperturbed equilibrium, and that the stochastic perturbation is in the order $O\left(\sqrt{\delta}\right)$, thus the Fokker-Planck operator corresponding to the deterministic and stochastic perturbation becomes

$$\mathscr{L}_{\mathbf{a}}p=-\nabla_{\mathbf{u}}\cdot\left(\mathbf{a}p\right),\quad \mathscr{L}_{\sigma}p=\frac{1}{2}\nabla\nabla_{\mathbf{u}}\cdot\left[\sigma\sigma^{T}p\right].$$

The equilibrium statistics and leading-order correction to the perturbation of some functional about the state variable $A\left(\mathbf{u}\right)$ can be formulated as an asymptotic expansion, $\overline{A\left(\mathbf{u}\right)}=\overline{A\left(\mathbf{u}\right)}_{\text{eq}}+\delta\overline{A\left(\mathbf{u}\right)}\left(t\right)+O\left(\delta^{2}\right)$, with

$$\overline{A\left(\mathbf{u}\right)}_{\text{eq}}=\int A\left(\mathbf{u}\right)p_{\text{eq}}\left(\mathbf{u}\right)d\mathbf{u},\quad \delta\overline{A\left(\mathbf{u}\right)}\left(t\right)=\int_{0}^{t}\mathscr{R}_{A}\left(t-s\right)\delta f\left(s\right)ds. \tag{12}$$

Above the 'overbar' denotes the statistical average under the solution from Fokker-Planck equation. $\mathscr{R}_{A}\left(t\right)$ is the *linear response operator to perturbations* according to the functional A, which is calculated through correlation functions in the unperturbed climate only

$$\mathscr{R}_{A}\left(t\right)=\overline{A\left(\mathbf{u}\left(t\right)\right)B\left(\mathbf{u}\left(0\right)\right)}_{\text{eq}},\ B\left(\mathbf{u}\right)=\frac{\left(\mathscr{L}_{\mathbf{a}}+\mathscr{L}_{\sigma}\right)p_{\text{eq}}}{p_{\text{eq}}}. \tag{13}$$

Note that even though in general the linear response operator is difficult to calculate considering the complicated and unaccessible equilibrium distribution. A convenient way to get accurate estimation about the linear response operator is from the Gaussian approximation about each spectral mode and assume independence between modes with different wavenumbers (Majda et al. 2005, 2010). The simple form of the quasi-Gaussian closure, p_{eq}, makes it possible for the development of exact formulation about the FDT algorithm and linear response operator (see Appendix B for the explicit forms of the linear response operators for the two-layer equations).

b. Low-dimensional reduced-order closure models

In developing reduced-order models, we concentrate on the first M dominant modes, $|\mathbf{k}| \leq M, M \ll N$, that cover the most energetic directions in the system. The nonlinear term in (5) always includes interactions between modes in a wide spectrum through the triads $\mathbf{k} = \mathbf{m} + \mathbf{n}$. Thus the (unresolved) less energetic high wavenumber modes ($|\mathbf{k}| > M$) could be important for the final energy spectrum in low wavenumber modes ($|\mathbf{k}| \leq M$) due to the strong backward cascade of energy through these nonlinear triad interactions. Therefore careful calibration about the small-scale unresolved nonlinear feedbacks in the resolved large-scale modes forms the central issue in the construction of low-dimensional truncated reduced-order models to achieve both computational accuracy and efficiency.

From the exact statistical equation (7), the linear dynamics in the two-layer equations are decoupled into a 2×2 blocked-diagonal system with interactions only inside the barotropic and baroclinic mode within the same wavenumber. The statistical modes with different wavenumbers are coupled only through the nonlinear interactions, Q_F, in third-order moments. In the development of reduced-order models, this becomes the most expensive but crucial part to estimate. Therefore a judicious estimation about these nonlinear interaction terms is the major task in designing the low-order schemes. The basic idea can be viewed as replacing the expensive nonlinear interactions in the small-scale with proper additional nonlinear damping and noise as in Majda and Qi (2016); Qi and Majda (2016). Additional damping serves as the stabilizing effects balancing on the linearly unstable modes, while adding additional noise excitation models the energy received on the stable modes. Considering all these aspects, the reduced-order models can be formulated in the forms of the 2×2 blocks about barotropic and baroclinic pairs with the same wavenumber as

$$\frac{dR_{M,\mathbf{k}}}{dt}=\left(\mathscr{L}_{\mathbf{k}}-\mathscr{D}_{\mathbf{k}}\right)R_{M,\mathbf{k}}+Q_{M,\mathbf{k}}+Q_{\sigma,\mathbf{k}}+c.c.,\quad |\mathbf{k}|\leq M. \tag{14}$$

The above equations are only solved for the resolved modes among wavenumbers $1\leq|\mathbf{k}|\leq M\ll N$. Comparing with the exact formulation (7), the imperfect model approximation comes from the nonlinear flux $Q_{M,\mathbf{k}}$, which characterizes the unresolved higher-order interactions due to the quadratic nonlinear effects. The major interest is to see whether we can construct proper reduced low-order approximation model (14) to capture the model sensitivities when various kinds of model perturbations are applied through the forcing perturbation from $Q_{\sigma,\mathbf{k}}$.

In general in the original dynamics, the nonlinear flux $Q_{F,\mathbf{k}}$ describes the energy transfer from the unstable subspace to the stable one through higher-order interactions. As described in Qi and Majda (2016) for one-layer barotropic flow, the low-order approximation of this nonlinear flux is through additional damping and noise by splitting this operator into two separate components, $Q_{M,\mathbf{k}}(E)=Q^{+}_{M,\mathbf{k}}(E)+Q^{-}_{M,\mathbf{k}}(E)$. The low-order correction made in $Q_{M,\mathbf{k}}$ is only constructed from the first two order of statistics. The next task is to propose proper forms to calibrate the nonlinear flux forms using additional damping in Q^{-}_{M} and additional noise in Q^{+}_{M}.

Reduced-Order Statistical Energy Closure

A preferred approach for the nonlinear flux $Q_{M,\mathbf{k}}$ combining both the detailed model energy mechanism and control over model sensitivity is proposed in the form

$$Q_{M,\mathbf{k}}=Q^{-}_{M,\mathbf{k}}+Q^{+}_{M,\mathbf{k}}=f_1(E)\left[-\left(N_{M,\mathbf{k},\mathrm{eq}}+d_M\right)R_{M,\mathbf{k}}\right]+f_2(E)\left[Q^{+}_{F,\mathbf{k},\mathrm{eq}}+\sigma^2_{M,\mathbf{k}}\right]. \tag{15}$$

The closure form (15) consists of three indispensable components:

i) *higher-order corrections from equilibrium statistics*: in the first part of the correction $\left(N_{M,\mathbf{k},\mathrm{eq}}, Q^{+}_{F,\mathbf{k},\mathrm{eq}}\right)$, unperturbed equilibrium statistics in the nonlinear flux are used to calibrate the higher-order moments as additional energy sink and source. The true equilibrium higher-order flux can be calculated without error from first and second order moments in $R_{\mathbf{k},\mathrm{eq}}$ from the unperturbed true dynamics (7) with $Q_{\sigma,\mathbf{k}} \equiv 0$ in steady state

$$Q_{F,\mathbf{k},\mathrm{eq}} = Q^{-}_{F,\mathbf{k},\mathrm{eq}} + Q^{+}_{F,\mathbf{k},\mathrm{eq}} = -\left(\mathscr{L}_{\mathbf{k}} - \mathscr{D}_{\mathbf{k}}\right) R_{\mathbf{k},\mathrm{eq}} + c.c., \quad N_{M,\mathbf{k},\mathrm{eq}} = \frac{1}{2} Q^{-}_{F,\mathbf{k},\mathrm{eq}} R^{-1}_{\mathbf{k},\mathrm{eq}}. \tag{16}$$

$Q^{-}_{F,\mathrm{eq}}, Q^{+}_{F,\mathrm{eq}}$ are the negative and positive definite components in the unperturbed equilibrium nonlinear flux $Q_{F,\mathrm{eq}}$. Since exact model statistics are used in the imperfect model approximations, the true mechanism in the nonlinear energy transfer can be modeled under this first correction form. This is the similar idea used for measuring higher-order interactions in Sapsis and Majda (2013a,b), while more sophisticated and expensive calibrations are required to make that model work;

ii) *additional damping and noise to model nonlinear flux*: the above closure by using equilibrium information for nonlinear flux is not sufficient for accurate prediction in the reduced-order methods since the scheme is only marginally stable and the energy transferring mechanism may change with large deviation from the equilibrium case when external perturbations are applied. We propose the additional damping and noise $\left(d_M, \sigma^2_{M,\mathbf{k}}\right)$ as from Majda and Qi (2016); Qi and Majda (2016) for further corrections in the form

$$Q^{\mathrm{add}}_{M,\mathbf{k}} = -d_M R_{M,\mathbf{k}} + \sigma^2_{M,\mathbf{k}}, \quad d_M = \begin{bmatrix} d_{M,\psi} & i\omega_M \\ -i\omega_M & d_{M,\tau} \end{bmatrix}. \tag{17}$$

Here specifically for the two-layer system, we introduce the additional damping operator d_M with different damping rates in the barotropic mode, $d_{M,\psi}$, and baroclinic mode, $d_{M,\tau}$. The off-diagonal parameter ω_M introduces additional calibration for the internal energy transfer between the barotropic and baroclinic mode;

iii) *statistical energy scaling to improve model sensitivity*: Still note that we add these additional parameters regardless of the true nonlinear perturbed energy mechanism where only unperturbed equilibrium statistics are used. To capture the responses to a specific perturbation forcing, it is better to make the imperfect model parameters change adaptively according to the total energy structure. Considering this, the additional damping and noise corrections are scaled with factors $f_1(E), f_2(E)$ related with the total statistical energy E in (9) as

$$f_1(E) = \left(\frac{E}{E_{\text{eq}}}\right)^{1/2}, \quad f_2(E) = \left(\frac{E}{E_{\text{eq}}}\right)^{3/2}. \tag{18}$$

In the positive-definite part $Q_{F,\text{eq}}^{+} + \sigma_M^2$, it calibrates the rate of energy injected into the spectral mode due to nonlinear effect. The term multiplying noise scales with $E^{3/2}$ so that the corrections to higher statistics keep consistent in scaling dimension with the third-order moment approximations; In the negative damping rate $N_{M,\text{eq}} - d_M$, the scaling function is used to characterize the amount of energy that flows out the spectral mode due to nonlinear interactions. Still scaling with a square-root for the total energy $E^{1/2}$ is applied for this damping rate to make it consistent in scaling dimension.

Next we discuss the detailed calibration about the nonlinear flux approximations. Two steps of model calibration should be considered: i) *the equilibrium consistency* that the reduced model will converge to the true equilibrium statistics as no perturbations are added; ii) *model sensitivity* by blending statistical response and information theory so that the imperfect model can capture the responses to various kinds of perturbations as the system is perturbed. Construction (16) guarantees equilibrium consistency using the true equilibrium model nonlinear flux structure. On the other hand, to improve model sensitivity, the linear response operators with information metric are used to find optimal parameters from the correction part in (17).

1) Climate consistency

In designing the reduced-order models, equilibrium consistency should be guaranteed in the first place in the unperturbed climate. That is, the same final unperturbed statistical equilibrium $R_{\mathbf{k},\mathrm{eq}}$ should be recovered from the reduced-order models $R_{M,\mathbf{k}}$ in each resolved mode $\mathbf{k}$. Comparing the true statistical equation (7) with the reduced-order model (14), time derivatives about the statistics on the left hand sides vanish in statistical steady state, thus climate consistency can be achieved only if we have exact recovery of the estimation in the nonlinear flux term. Specifically, it requires that the model nonlinear flux correction term (15) converges to the truth, $Q_M \rightarrow Q_{F,\mathrm{eq}}$, when no external perturbation is added, $Q_\sigma = 0$. Under this condition in steady state the reduced-order model (14) goes to the true unperturbed statistics

$$0 = (\mathscr{L}_{\mathbf{k}} - \mathscr{D}_{\mathbf{k}}) R_{M,\mathbf{k}} + Q_{F,\mathbf{k},\mathrm{eq}} + c.c. \ \rightarrow \ R_{M,\mathbf{k}} = R_{\mathbf{k},\mathrm{eq}}.$$

In construction the first component $\left(N_{M,\mathbf{k},\mathrm{eq}}, Q^{+}_{F,\mathbf{k},\mathrm{eq}}\right)$ comes from the true equilibrium statistics. This part will be automatically equal to the true nonlinear flux in equilibrium. Thus climate consistency requires that the second component correction makes no contribution in the unperturbed case, and no further correction in the scaling functionals. That is,

$$\sigma^2_{M,\mathbf{k}} = d_M R_{M,\mathbf{k},\mathrm{eq}}, \quad f_1\left(E_{\mathrm{eq}}\right) = 1, \ f_2\left(E_{\mathrm{eq}}\right) = 1. \tag{19}$$

By choosing parameters according to (19), the climate consistency for the imperfect reduced-order models in (14) in the unperturbed equilibrium is guaranteed. In addition, we still leave one controlling parameter d_M for the freedom to tune the imperfect model performance in both barotropic and baroclinic mode, considering that climate consistency is only the necessary but not sufficient condition for good model prediction (Majda and Gershgorin 2011).

2) Model calibration blending statistical response and information theory

Next we try to find a unified way to achieve the optimal model parameters d_M such that the imperfect models can maintain high performance for various kinds of external perturbations. Accurate modeling about the model sensitivity to various external perturbations requires the imperfect reduced-order models to correctly reflect the true system's "memory" about its previous states. Following the idea in Majda and Gershgorin (2011); Majda and Qi (2016), it is noticed that the linear response operator $\mathscr{R}_A$ in (13) can characterize the model sensitivity involving the nonlinear effects in the system regardless of the specific forms of the external perturbations. The optimal imperfect model parameter thus can be achieved by measuring the linear response operator under the unbiased information metric.

Information-theoretical framework to measure the linear responses In this training phase, we try to find the optimal model parameters d_M by comparing the linear response operators from the true system and imperfect approximation model. The true model linear response operator can be calculated from (13) with the quasi-Gaussian closure which is detailed in Appendix B, and the reduced-order model response operators are calculated from the kicked response strategy (Majda and Qi 2016; Qi and Majda 2016). The distance between these two operators can be calculated through the information metric from Kullback and Leibler (1951); Majda and Gershgorin (2011) which offers an unbiased and invariant measure for model distributions

$$\begin{aligned}\mathscr{P}\left(\pi_\delta,\pi_\delta^M\right) &= \mathscr{S}\left(\pi_{G,\delta}\right)-\mathscr{S}\left(\pi_\delta\right)\\ &\quad +\frac{1}{4}\sum_{\mathbf{k}}R_{\mathbf{k}}^{-2}\left(\delta R_{\mathbf{k}}-\delta R_{M,\mathbf{k}}\right)^2+O\left(\delta^3\right).\end{aligned} \tag{20}$$

The first row above is the inherent information barrier due to the second-order closure approximation; and the last row is the dispersion error for calibrating the linear responses in the first two order of moments, $\delta R_{\mathbf{k}}$.

Correction through total statistical energy In the previous calibrations, we just consider the equilibrium statistics without any perturbed model measurements considered. To capture the responses to a specific perturbation forcing, it is better to make the imperfect model parameters change adaptively according to the total energy structure. In the closure form (15), two additional scaling factors, f_1, f_2, are introduced to further quantify the nonlinear energy flux in and out the spectral modes due to the nonlinear interactions. We propose the dynamical corrections with the total statistical energy E as in the forms (18). This total energy correction introduces global information into each spectral mode so the nonlinear energy transfer can be better characterized in the imperfect model, while solving only one additional scalar equation is the only additional cost in computation. The scaling factor from $E(t)$ introduces nonlinear global effects into the additional damping and noise corrections in each mode.

One further difficulty is about solving this statistical energy equation in (10) since only the first few low-wavenumber modes are resolved. The strategy here is to run the approximated equation instead and again use the equilibrium steady state statistics to estimate the unresolved part. Therefore the dynamical equation we need to run becomes

$$\frac{dE_M}{dt} + k_d^2 U \sum_{|\mathbf{k}|\leq M} ik_x \overline{\psi_{\mathbf{k}}^* \tau_{\mathbf{k}}} = -\kappa E_M + \frac{\kappa}{2} \sum_{|\mathbf{k}|\leq M} \left[k_d^2 \overline{|\tau_{\mathbf{k}}|^2} + 2|\mathbf{k}|^2 \mathfrak{Re}\overline{\psi_{\mathbf{k}}^* \tau_{\mathbf{k}}} \right] + \frac{E_M}{E_{M,\mathrm{eq}}} Q_\infty + Q_\sigma. \quad (21)$$

Above in the model equation, only the resolved part is calculated explicitly and the unresolved component Q_∞ is from the equilibrium statistics and again scaled with the statistical energy. In explicit form we can calculate

$$Q_\infty = \left[k_d^2 U \sum_{|\mathbf{k}|\leq M} ik_x \overline{\psi_{\mathbf{k}}^* \tau_{\mathbf{k}}} + \kappa E_M - \frac{\kappa}{2} \sum_{|\mathbf{k}|\leq M} \left(k_d^2 \overline{|\tau_{\mathbf{k}}|^2} + 2 |\mathbf{k}|^2 \overline{\psi_{\mathbf{k}}^* \tau_{\mathbf{k}}} \right) \right]_{\text{eq}}.$$

Therefore the solution of the above equation (21) can be used as an approximation of the total energy E of the system and a more feasible scaling factor to calibration the nonlinear flux including all the external perturbation forms. The additional computational expense for solving the scalar equation (21) is fairly low.

In summary, we approximate high-order nonlinear energy flux in the true system with an additional damping terms Q_M^- and the additional noise Q_M^+ consisting of two components. The first component calibrates the nonlinear energy transfers through the true equilibrium information, thus the model can reflect the true energy mechanism; and the second component offers better control for the model sensitivity, thus we can seek the optimal parameters through a training process. Model equilibrium consistency is guaranteed through this construction. Model sensitivity can simply be controlled by the constant parameter d_M. Two more scaling coefficients, f_1 and f_2 with total statistical energy, are introduced to further improve the model sensitivity to external perturbations.

c. Summary of the Reduced-Order Statistical Energy Closure *algorithm*

We summarize the low-dimensional reduced-order statistical closure algorithm with calibration from total statistical energy and linear response theory (Majda 2015; Majda and Qi 2016). The general reduced-order model algorithm is split into two separated steps of a training phase and a prediction phase. The training phase is used to improve model sensitivity by tuning the imperfect model parameter using only unperturbed climate statistics for the linear response operator. Then the optimal parameter can be applied for predicting model responses to different kinds of external perturbations.

Algorithm 1 *(Reduced-order statistical closure model for two-layer baroclinic turbulence)*

Decide the low-dimensional subspace $\mathbb{R}^M$ *spanned by orthonormal basis* $\{\mathbf{e}_\mathbf{k}\}_{|\mathbf{k}|=-M}^{M}$ *covering the regime with largest variability (energy) in the spectrum. Set up statistical dynamical equations (14) by Galerkin projecting the original equations to the resolved subspace* $\mathbb{R}^M$ *for* $1 \leq |\mathbf{k}| \leq M$*, as well as the statistical energy equation (21) to get the total statistical energy* E_M *in the system. The reduced-order method can be carried out in two steps with a calibration phase and a prediction phase:*

- *Calibration step:*
  - *Construct low-order approximation of the nonlinear flux in the statistical equations using the statistical energy closure proposed in (15) consistent with the equilibrium climate;*
  - *Compute the true linear response operator from the unperturbed equilibrium statistics, and calculate the imperfect model predicted linear response operator from proper estimation strategies (using formulas shown in Appendix B);*
  - *Determine the imperfect model parameter values through minimizing the information distance (20) between linear response operators from true equilibrium statistics and imperfect model approximation;*
- *Prediction step:*

– *Use the optimal tuned parameters achieved from the previous step in the reduced-order model to get statistical responses of the state variables of interest in principal directions with all kinds of specific external perturbations.*

Note that in the calibration step in the algorithm, only the unperturbed statistics in equilibrium are required. Thus this offers the optimal model parameters that are ideally valid for all kinds of specific forcing perturbation forms. With the help of the linear response operator we are able to find a unified way to tune the imperfect model parameters and avoid the exhausting and impractical process to tune the models each time with different kinds of perturbations.

4. Reduced-order models with homogeneous mean flow

In this section, we test the prediction skill of the reduced-order model for the two-layer QG turbulence in both representative ocean and atmosphere regimes. Distinct turbulent structures can be produced at different latitudes as the β-effect changes. In high latitude case (strongly supercritical), homogeneous statistical can be generated, while in low/mid latitude case (weakly supercritical), anisotropic jets are representative features that can always be observed. In this section we focus on the high latitude ocean and atmosphere regimes with homogeneous statistics, and the imperfect model skill in capturing inhomogeneous structures will be discussed in next section.

Set-up of numerical simulations

In numerical simulations, the true statistics is calculated by a pseudo-spectra code by resolving the two-layer equations (1) with 128 spectral modes zonally and meridionally, corresponding to $256\times256\times2$ grid points in total. In the reduced-order methods, only the large-scale modes $|\mathbf{k}|\leq 10$ are resolved, which is about 0.15% of the full model resolution. For the nonlinear advection terms a standard 3/2-rule is applied to get rid of aliasing error. The time integration is through the standard 4th-order Runge-Kutta methods with time step $\Delta t = 5 \times 10^{-4}$ and $\Delta t = 5 \times 10^{-3}$ for ocean and atmosphere regime respectively, which is small enough to capture all the small-scale dynamics. Note that due to the much smaller Rossby deformation radius in the ocean regime, the system becomes more stiff and much smaller time step is required for the ocean case for stability. The time-series are recorded at every 20 or 10 time steps for ocean and atmosphere case, that is, we sample the data at every 0.01 or 0.05 time unit. We integrate the system up to a long time with $N = 3.5 \times 10^5$ time steps with the first 5000 steps skipped in the calculation of model statistics.

EXTERNAL FORCING IN STOCHASTIC AND DETERMINISTIC COMPONENT

The forcing perturbations are expressed in the barotropic and baroclinic mode individually as in (2). The barotropic perturbation can be used to describe the penetrated forcing through the flow surface independent of depth; while the baroclinic perturbation can represent the effects from radiative heating and baroclinic stirring. In our testing cases, the stochastic forcing is represented as a random Gaussian process, where only the variance spectrum in wavenumber needs to be prescribed; and the deterministic forcing is introduced through a perturbation in the vertical shear as follows:

- The amplitude of the *stochastic forcing* is introduced according to the equilibrium energy so that

$$\sigma_{\psi,\mathbf{k}}^2 = \delta\sigma_0^2 \overline{\left|q_{\psi,\mathbf{k}}\right|^2}_{\mathrm{eq}}, \quad \sigma_{\tau,\mathbf{k}}^2 = \delta\sigma_0^2 \overline{\left|q_{\tau,\mathbf{k}}\right|^2}_{\mathrm{eq}}. \tag{22}$$

  σ_0 is a scaling variable to control the strength of the barotropic and baroclinic perturbations; $\overline{\left|q_{\psi,\mathbf{k}}\right|^2}_{\mathrm{eq}}, \overline{\left|q_{\tau,\mathbf{k}}\right|^2}_{\mathrm{eq}}$ are from the unperturbed equilibrium statistics of the vorticity so that the energy injected into each mode is balanced. Only modes in largest scales, $1 \leq |\mathbf{k}| \leq 10$, are perturbed, while the higher wavenumbers are kept unperturbed in the following numerical tests.

- The *deterministic forcing* is introduced through a perturbation in the background shear $U_\delta = U + \delta U$, so that the perturbation on the barotropic and baroclinic mode becomes

$$\delta f_{\psi,\mathbf{k}} = \delta U i k_x \left(-|\mathbf{k}|^2\right) \tau_{\mathbf{k}}, \quad \delta f_{\tau,\mathbf{k}} = \delta U i k_x \left(-|\mathbf{k}|^2 + k_d^2\right) \psi_{\mathbf{k}}. \tag{23}$$

  Still the perturbation strength is according to the structure in each barotropic and baroclinic mode so that the forcing is balanced. This deterministic perturbation due to the change in shear flow strength is then applied along the entire spectrum. This is the same perturbation form tested in Sapsis and Majda (2013a) with a more complicated set of closure methods.

The strong nonlinear interactions in the QG flow induce energy exchange between small and large scales even when only the large-scale modes are perturbed. The challenge in the reduced-order model is to predict the nonlinear responses to barotropic and baroclinic perturbations with only large-scale modes resolved.

a. True model statistics with homogeneous structure

In the first place, we demonstrate the true model statistics and energy structure. Parameters for high-latitude dynamical regimes are shown in Table 1. These parameters are chosen so that baroclinic instability is exhibited in a wide range of modes $\sqrt{\frac{\beta}{2U}} \leq |\mathbf{k}| \leq k_d$ with a turbulent cascade. The unstable waveband spectra from linear analysis in each regime are also listed in the last three columns of the table. The Ekman damping reduces the maximum growth rate while at the same time extends the spread of the unstable waveband. The ocean regime in general has a wider band of instability with more unstable small-scale (high wavenumber) modes and stronger growth rate compared with the atmosphere case. Due to the β-effect stopping the inverse energy cascade, the largest scales $|\mathbf{k}| < 2$ always stay (linearly) stable. Small hyperviscosity, $\nu = 1.2 \times 10^{-15}$ (ocean) or $\nu = 5 \times 10^{-15}$ (atmosphere), is added to both barotropic and baroclinic modes to dissipate the unresolved small-scale fluctuations.

In the simulations for the unperturbed system in high-latitude regimes, no external forcing is added in either deterministic or stochastic component. Figure 1 displays the two-layer flow structure in *high-latitude ocean regime.* The first row is the snapshots of the barotropic and baroclinic vorticity. Homogeneous structure can be observed in both cases while larger scale structures appear in the baroclinic mode. It is important to notice the strong correlation in the coherent structures in the barotropic and baroclinic field, illustrating the strong energy transfer between the two modes. The following part shows time-series of the energy in barotropic and baroclinic mode, $-\int \psi q_\psi, -\int \tau q_\tau$, as well as the potential energy, $\int k_d^2 \tau^2$, compared with the meridional heat flux, $k_d^2 U \int \psi_x \tau$. Baroclinic mode appears more active with larger energy in this ocean regime. In Figure 2 the results for the two-layer flow in *high-latitude atmosphere regime* are compared. One important feature here is the flow field alternating between blocked and unblocked regimes. In the stream functions, it can be observed that in the blocked regime, zonal flow is blocked and the field is restricted at separated regimes, while in the unblocked regime strong zonal flow can be observed. Strong meridional heat flux can be observed in the blocked regime while the flow is in state with lower energy and heat transfer rate in the zonal unblocked regime. In the atmosphere case, the barotropic energy is larger, while potential energy is dominant in the baroclinic energy. For further comparison, the zonally averaged mean flow fields $u = -\partial_y \psi$ in both regimes are shown in Figure 3. Again we observe homogeneous statistics in both fields while atmosphere regime show larger scale structures. Similar phenomena are observed in many other simulations about the two-layer flow (Harlim and Majda 2010; Vallis 2006; Treguier and Hua 1987; Grooms and Majda 2013).

To understand the energy mechanism in the true model, we check the instability and equilibrium statistical features in both ocean and atmosphere regimes. Each wavenumber includes the barotropic and baroclinic mode as a 2×2 block. The linear part, $(\mathscr{L}_{\mathbf{k}}-\mathscr{D}_{\mathbf{k}})\,R_{\mathbf{k}}$, in the original statistical equation (7) illustrates the stable and unstable subspace where baroclinic instability takes place. The nonlinear part, $Q_{F,\mathbf{k}}$, on the other hand, shows the nonlinear energy transfer mechanism through the triad modes $\mathbf{k}=\mathbf{m}+\mathbf{n}$ between different scales. In Figure 4, we compare the linear growth rate with dissipation and the eigenvalues from the nonlinear flux Q_F in both high-latitude ocean and atmosphere regimes. In both regimes we can observe that the most unstable linear modes take place in zonal direction (with $k_y=0$) and all the meridional modes ($k_x=0$) become stable due to the asymmetric dissipation effects. Correspondingly, the nonlinear flux Q_F has negative eigenvalues in the zonal modes (meaning outflow of energy due to nonlinear interactions) and positive eigenvalues in the meridional modes (meaning inflow of energy). Therefore the energy mechanism can be summarized as that the linear unstable modes increase in energy due to the positive growth rate while the nonlinear operator will transfer the additional energy to the stable modes (effectively as an additional damping) due to linear instability. Note the wavenumbers with largest linear growth rate takes place in smaller scales than the position of nonlinear flux wavenumber with the largest eigenvalues. This illustrates the backward cascade of energy to large scales along the energy spectra and transfer of baroclinic energy to barotropic modes in the largest scales. Comparing the ocean and atmosphere regime, it is also important to notice that the ocean regime contains a wider range of unstable modes with larger amplitude due to the relative large deformation frequency k_d, while in the atmosphere regime the strongest nonlinear energy transfers take place at $|\mathbf{k}|=1,2$.

The general steady state statistical structures in the spectral field are shown in Figure 5. As implied from the homogeneous statistics, the mean states stay in small values within fluctuation errors in both ocean and atmosphere regimes. From the energy spectra, one observation is that the potential energy is dominant in large scales in the baroclinic modes, and the kinetic baroclinic energy becomes more important in small scales. More statistical features of the two-layer system can be revealed by the autocorrelation functions and the marginal distributions in the most energetic modes shown in Figure 6 for ocean and atmosphere regime. In the ocean regime, all the modes are mixing quite rapidly with a fast decaying autocorrelation function. The marginal distributions in the principal modes all appear like Gaussian with comparable amount of energy in each mode in the selected modes. In comparison in the atmosphere regime, the first two modes appear strongly non-Gaussian containing much higher energy than the other ones. Also the first two dominant modes are mixing for a much longer time with oscillatory autocorrelation functions. Still even with Gaussian-like marginal distributions in the ocean case, nonlinear non-Gaussian features in higher-order moments are important for the reduced-order methods. Figure 7 displays the joint-distributions in the most energetic modes in the ocean (mode $(5,2)$ and $(5,3)$) and atmosphere (mode $(1,0)$ and $(0,1)$) regime. The first two rows show the joint-distribution in barotropic and baroclinic modes in the principal modes. And the second parts show the joint-distributions with different wavenumbers between barotropic and baroclinic modes. Within the same wavenumber $\mathbf{k}$, as we have observed in the snapshots, the barotropic and baroclinic modes are strongly correlated with skewed joint PDFs. Especially in the atmosphere case, non-Gaussian structures can be observed in the first two modes. However in the joint distributions between different wavenumbers, the modes appear decoupled and independent with each other. This further guarantees the assumption of homogeneous statistics as $\langle p_{\mathbf{m}} p_{\mathbf{n}} \rangle = 0, \mathbf{m} \neq \mathbf{n}$ in the high-latitude regime, and validates the feasibility of using quasi-Gaussian approximation in calculating the linear response operators as a 2×2 blocked system.

b. Testing reduced-order model in homogeneous regime

In the previous section we displayed the unperturbed statistical structures of the two-layer QG system in high-latitude regime with important nonlinear non-Gaussian features. The major task now is to test the reduced-order model skills in predicting statistical responses to both stochastic and deterministic forcing perturbations as prescribed in (22) and (23) using only low-order closures. Only the large-scale modes $|\mathbf{k}| < 10$ are calculated here, which cover the regime of most energetic directions. And to investigate the model sensitivity in each component, the perturbations in barotropic mode and baroclinic mode are applied individually in the tests. Three statistical quantities are of special importance in characterizing the two-layer system, that is, the barotropic energy, $\overline{\left|p_{\psi,k}\right|^2}$, baroclinic energy $\overline{\left|p_{\tau,k}\right|^2}$, and the heat flux $ik_x\overline{\psi_k^*\tau_k}$. Due to the homogeneous statistics as we have shown before, the mean states become zero and thus we can focus on the second-order variances in this situation. Therefore we will mainly check the reduced-order method's ability in capturing the responses in these key quantities. Like the Algorithm summarized in Section 3.c, the modeling process are decomposed into a training phase for finding optimal model parameters and a prediction phase for getting responses to various perturbations.

1) Training phase with linear response operator

Equilibrium consistency for the reduced-order method

In testing the reduced-order models, we need to first guarantee climate consistency with the true unperturbed equilibrium in statistical steady state. In the construction of low-order correction in Section 3.b, higher-order statistics from equilibrium are combined with additional damping and noise corrections. It needs to be emphasized that neither the additional damping and noise (17) nor the equilibrium high-order correction (16) is stable on its own even with the climate consistency satisfied in (19). Due to the baroclinic instability in the linear operator, energy in the unstable subspace will increase and finally diverge from the true model climate. Instead by combining (17) and (16) to form the blended approach in (15), climate consistency can always be reached with exact recovery of variance in each mode as illustrated in Section 3.b. To further confirm the equilibrium consistency numerically, Figure 8 shows the steady state energy spectra from the reduced-order model together with the time convergence in total variance. Exact recovery in each individual mode as well as the total variance is observed in the combined scheme.

TUNING IMPERFECT MODEL RESPONSES THROUGH LINEAR RESPONSE THEORY

In the training phase before the prediction step, the optimal model parameters $d_M = \left(d_{M,\psi}, d_{M,\tau}\right)$ are calibrated through the information-theoretic framework (Majda and Qi 2016; Majda and Gershgorin 2011) combining the statistical response operator (13) and information metric (20). The strategies to get the linear response operator in the true signal and the reduced-order model are detailed in Appendix B. As an example, Figure 9 shows the linear response operators from the truth and imperfect model kicked-response in the high-latitude ocean regime with a stochastic perturbation in the barotropic mode. Since the system is strongly mixing in this high-latitude ocean regime, the operators all decay to zero quite rapidly. The reduced-order model only uses first two moments to estimate the higher-order interactions, thus some of the nonlinear structure in the beginning is missed. Nevertheless the imperfect closure model gets desirable approximation for these linear response operators in these leading modes.

In Figure 10 the tuning process by minimizing the information error in the resolved subspace as the model parameters d_M changes in value is displayed. To illustrate the effects from the total statistical energy correction in (18), the errors with and without the *energy scaling factor,* $f_1(E), f_2(E)$, are compared. In the right part for the method without using the scaling factor, larger information errors appear uniformly among the entire range of parameter values and it is difficult to improve the model prediction skill by only tuning the model parameters. Whereas with the proper energy correction, the information error can be effectively reduced with a wide parameter regime with small information errors as shown on the left, which implies the robustness of the method. Note again in this training phase only unperturbed equilibrium statistics are used without the specific perturbation forms, thus the method with optimal parameters can be used to predict system responses to various kinds of specific external forcings. As a further comparison, we show the reduced-order model predictions and information error with and without statistical energy correction in a typical case by perturbing the barotropic mode with stochastic noise in the ocean regime. This shows the essential role of the scaling factor to improve model sensitivity. Without the correction from total statistical energy, the response energy spectrum is highly underestimated with much larger information error compared with the method with energy correction due to the insufficient characterization in the higher-order interactions. The statistical energy correction then will always be applied in the following parts.

2) PREDICTION SKILL OF REDUCED-ORDER MODEL

MODEL RESPONSES TO STOCHASTIC FORCING IN BAROTROPIC AND BAROCLINIC MODE

In this first place, we test the model sensitivity to random stochastic perturbations as described in (22). We consider the perturbations in barotropic and baroclinic mode individually so that the contributions from each component can be identified. Usually, the baroclinic energy transfers to barotropic modes in the large scales and the nonlinear energy cascade alters the energy structure in the entire spectrum despite only the large scale modes are perturbed. The challenge here is whether the nonlinear responses can be captured with accuracy using reduced-order models where only corrections from low-order moments (that is, mean and variance) are used.

The high-latitude ocean regime responses in barotropic and baroclinic energy and heat flux in large-scale wavenumbers to stochastic perturbations are first shown in Figure 11. The perturbation amplitude is chosen as $\delta\sigma_0^2 = 0.5$ of the equilibrium energy in the stochastic forcing (22) so that the response is large and nonlinear. We compare the responses in perturbing only the barotropic mode and baroclinic mode. The most energetic and most sensitive scales take place at wavenumbers $|\mathbf{k}| = 4,5,6$. Both barotropic and baroclinic perturbations can lead to large changes in a wide spectrum in both barotropic and baroclinic component due to the strong coupling between the modes. In the reduced-order methods, only the first large-scale modes $|\mathbf{k}| < 10$ are resolved, while the responses in these dominant modes are all captured with accuracy in both perturbation cases though the complicated higher-order interactions with small-scale modes are not computed explicitly. Further the time-series with the total statistical energy from the equation (21) are compared. The dashed black lines mark the level of energy in unperturbed and perturbed case. In this regime, the total statistical energy can also be recovered exactly with little error. This in turn explains the high skill of the reduced-order models in predicting this regime. Instead, if we only consider the energy in the resolved subspace shown by blue lines, a large gap can be observed compared with the total energy. Figure 12 shows the results in the high-latitude atmosphere regime. Alternating blocked and unblocked structures appear in this regime and generate quite complicated statistical features. The leading mode $|\mathbf{k}| = 1$ contains most of the energy and becomes highly sensitive to perturbations. The reduced-order method keeps the skill in capturing the responses in the most sensitive directions in this difficult regime. Also it is observed that the baroclinic perturbation case becomes a little less accurate in both spectra and total statistical energy. This might be due to the stronger nonlinear energy interactions from baroclinic to barotropic mode.

A further test requires to check the model's robustness in predicting perturbations with different amplitudes. Figure 13 displays the prediction results with changing stochastic forcing amplitude

$\delta\sigma_0^2$ in the barotropic modes. The reduced-order model maintains the skill in predicting responses with various forcing strength, and the nonlinear trends in the total resolved barotropic and baroclinic energy as well as the heat flux are captured compared with the linear prediction in the FDT shown by dashed lines.

MODEL RESPONSES TO THE PERTURBED MEAN SHEAR δU

In checking the model responses to deterministic forcing, we introduce the forcing perturbation by changing the background jet strength U as in (23). The same perturbation is tested in Sapsis and Majda (2013a) for a more complicated reduced-order modified quasi-Gaussian closure (RoMQG), and we test the same perturbation form here under our systematic reduced-order modeling framework. Note that the deterministic perturbation in (23) forms a more difficult test case compared with the stochastic forcing (22) because the forcing is applied along all wavenumbers with stronger mean-fluctuation interactions involved. On the other hand, for the reduced order methods, only the perturbations at the limited resolved modes are quantified. This gives the inherent difficulty for applying the reduced order models to this kind of perturbations since we have no knowledge of the unresolved modes where large amount of energy is contained. Therefore the statistical energy equation (21) plays a crucial role.

The results with mean flow perturbations $\delta U = \pm 0.05$ in the ocean regime and perturbations $\delta U = 0.02, -0.01$ in the atmosphere regime are shown in Figure 14 and 15 separately. The perturbation accounts for about 5%-10% of the original shear strength U, and the corresponding responses in both energy and heat flux spectra are large due to this global perturbation at every wavenumber and nonlinear energy cascade. In the ocean regime, a wide waveband of modes $|\mathbf{k}| = 3,4,5,6$ becomes sensitive to the perturbations; while in the atmosphere regime, the first dominant mode $|\mathbf{k}| = 1$ is especially sensitive according to even small perturbations. This illustrates the strong nonlinear interactions between the high and low wavenumber modes. The reduced-order method displays uniform skill in capturing the sensitive responses in the large-scale modes for both positive and negative perturbation cases with only first 10×10 spectral modes resolved compared with the 256×256 full resolution model.

5. Reduced-order model with inhomogeneous jet flow

In mid or low latitude regimes, both the ocean and atmosphere are distinctly inhomogeneous on large scales. The existence of large-amplitude meandering zonal jets in these regimes suggests regional metastable equilibria, while the large-scale forced perturbations may lead to regular or irregular fluctuations in some extent. Following the same systematic information-theoretic procedure, we test the prediction skill of the reduced-order method in this inhomogeneous regime with anisotropic jets in this section.

a. True model results with anisotropic jets

The set-up of the two-layer system in this low/mid latitude case is kept exactly the same as previous in Section 4. The parameters used for low/mid latitude ocean and atmosphere regime are listed in Table 2. Larger β-effect is applied in this regime, and the Ekman friction has a smaller value. Compared with the high latitude case, the first unstable wavenumber takes place at larger values in smaller scales, and the linear growth rate is weaker than that in the high latitude.

Flow snapshots in both ocean and atmosphere regime in low/mid latitude are plotted in Figure 16. In the ocean regime, multiple steady jets can be observed and the jets can be persistent for a long time; in the atmosphere regime, there appears one dominant jet meandering in time. The jet structures are illustrated in more detail in Figure 17 for the time-series of the zonally average mean flow, $u = -\partial_y \psi$. Linear analysis and nonlinear flux eigenvalues can be found in Figure 18. In this low/mid latitude case, especially for the ocean regime, due to the strong zonal jets in wavenumber $k_y = 6$, zonal modes with $k_x = 5,6$ become active due to the nonlinear interactions.

Unperturbed statistical steady state energy spectra in mean and variance are displayed in Figure 19. The mean states stay in small values except for the active meridional modes in both ocean and atmosphere regimes. One dominant mode ($k_y = 6$ for ocean and $k_y = 1$ for atmosphere) appears representing the zonal jet structure. This illustrates the stronger mean-fluctuation interactions in this regime, and a more challenging test case for the reduced-order schemes. Most of the energy and variances are contained in the first 20 modes in both barotropic and baroclinic component in the ocean regime, while in the atmosphere regime the first mode contains most energy of the system. The autocorrelation functions and the marginal distributions in the most energetic modes are also shown in Figure 20 for low/mid latitude ocean and atmosphere regime. In the ocean regime, all the modes are mixing relatively faster with highly oscillating autocorrelation functions. The marginal distributions in the principal modes all appear like Gaussian with comparable amount of energy in each dominant mode with zonal wavenumber $k_x = 6$. In comparison in the atmosphere regime, there exist two meridional modes $(0,1)$ and $(0,2)$ with highly non-Gaussian structure and extremely long decorrelation time. The other energetic modes are mixing relatively faster in the autocorrelation functions, and the distributions appear more like Gaussian. This extremely long mixing time in the meridional modes illustrates the persistent single zonal jet in long time scale. Still weaker stochasticity with strong non-Gaussian features is generated in the low/mid-latitude regime making it a quite challenging regime for the statistical closure methods.

b. Predictions with reduced-order model

Again we check the reduced-order model skill in capture stochastic perturbations in this inhomogeneous situation. We propose the random forcing perturbation with variance proportional to the unperturbed equilibrium steady state statistics as in (22), and only the large-scale modes, $1 \leq |\mathbf{k}| \leq 10$, are perturbed. In the atmosphere regime, one important observation is that with small random perturbation added, one persistent single zonal jet structure is generated like the assumed radiative equilibrium in Pavan and Held (1996). It is observed that similar structure can be generated through a random forcing in the two-layer model. Considering these observations, we use the following test cases for testing the reduced-order methods for low/mid latitude ocean and atmosphere regimes:

- In the ocean regime, we use the case with no stochastic forcing $\sigma_0^2 = 0$ as the unperturbed equilibrium climate, and the perturbed case is to use random perturbation with noise $\sigma_0^2 = 0.2$;
- In the atmosphere regime, we use the case with small random forcing $\sigma_0^2 = 0.2$ as the unperturbed equilibrium climate, and the perturbed case is to use stronger random forcing with noise $\sigma_0^2 = 0.4$.

Like the previous case, the perturbation amplitude is large enough to generate strong nonlinear responses in the statistical energy in each mode. In the reduced-order model, only the modes with wavenumbers $|\mathbf{k}| \leq 10$ are calculated. Thus the resolved subspace is 10^2 compared with the full dimensionality of the system of 256^2. Note from the stability analysis in Table 2, the resolved spectrum is even smaller than the total number of unstable modes, that is, there are also unresolved unstable modes that have positive growth rate. Again, the first step should make sure the reduced methods keep the ability to reproduce the exact statistics in the unperturbed equilibrium, and get optimal reduced-order model parameters in the training phase. The exact same procedure as in Section 4.b.1 can be followed and we neglect the detailed tuning regime results here.

In Figure 21 and 22, we compare the model responses in both low/mid-latitude ocean and atmosphere regimes. In this inhomogeneous regime with anisotropic jets, the statistical variables combine the responses in the mean and variance, $\overline{p_{1,\mathbf{k}}^{*}p_{2,\mathbf{k}}}=\bar{p}_{1,\mathbf{k}}^{*}\bar{p}_{2,\mathbf{k}}+\overline{p_{1,\mathbf{k}}^{\prime *}p_{2,\mathbf{k}}^{\prime}}$, to display the total effect from the perturbation. In the ocean regime, we use the unperturbed case with no random forcing, and for the perturbed case forcing is added with white noise variance $\sigma_0^2=0.2$. The dominant mode with largest sensitivity is at wavenumber $|\mathbf{k}|=6$ due to the zonal jet structure. The sensitivity is captured with accuracy in the reduced-order method. Also we compare the time evolution of the total resolved energy and heat flux. The prediction is also good with small error. In the atmosphere regime, the unperturbed case is with random forcing $\sigma_0^2=0.2$ and the perturbation is added with $\sigma_0^2=0.4$. The first mode $\mathbf{k}=(0,1)$ has a large mean state representing the zonal mean flow. Thus $|\mathbf{k}|=1$ mode gets the largest statistical energy and is most sensitive to perturbations. One important feature is the large change in the heat flux in the first two modes, representing the exchange of energy in the dominant barotropic and baroclinic mode. Still the responses can be captured with accuracy in each mode in the spectra as well as the total energy and heat flux profile with only 10^2 modes resolved. Note that in both cases, the heat flux is weak due to the strong zonal jets.

6. Summary

In this paper, we discuss the development of efficient low-dimensional reduced-order models for the two-layer quasi-geostrophic turbulence to capture statistical responses to external perturbations in various dynamical regimes. The computational cost is reduced through a systematic approximation about the expensive nonlinear higher-order interactions following the generic framework developed in Majda and Qi (2016); Qi and Majda (2016). Additional nonlinear damping and noise corrections are proposed to replace the third-order moments, and the model errors are calibrated through an information-theoretic framework using information theory as in Majda and Gershgorin (2011). Two successive steps are then carried out in the algorithm concerning model consistency in unperturbed equilibrium and sensitivity to external perturbations. Note that imperfect models with statistical equilibrium fidelity still suffer inherent information barrier in model sensitivity to perturbations, linear response operators involving only unperturbed equilibrium statistics are proposed to fit the model parameters in a training phase to achieve optimal model prediction skill. The imperfect model sensitivity is further improved using the total statistical energy equation (Majda 2015) for the two-layer baroclinic flow. The total statistical energy characterizes the entire energy structure in the system according to specific external perturbations despite the inhomogeneity, and introduces one global scaling factor that offers more detailed model calibration for the unresolved higher-order interactions. The additional computational cost only requires solving one additional scalar dynamical equation.

The feasibility of the reduced-order models is tested on various dynamical regimes in the two-layer QG system in response to both stochastic and deterministic perturbations. Distinct statistical structures can be generated as the model parameters change. Homogeneous statistics with zero mean state can be observed in the high-latitude regime, while anisotropic jets become representative in the low/mid-latitude regime (Grooms and Majda 2013; Panetta 1993; Treguier and Hua 1987). Also atmosphere regime shows more large-scale structures and ocean regime contains more small-scale eddies in the vorticity field. These dynamical regimes offer desirable testbeds for testing the robustness of the reduced-order model skill in treating different types of statistical features. To simulate the various external effects that drive the atmosphere/ocean flow, the forcing perturbation is decomposed into the barotropic and baroclinic component. The reduced-order method is developed in the uniform framework for predicting all the dynamical regimes with different kinds of external forcing and perturbation. High prediction skill is displayed in the reduced-order model among the various test regimes in capturing model responses for both the mean and variance in principal modes with only about 0.15% of the full resolution modes calculated explicitly. In contrast, FDT performs well in the linear regime with small perturbation amplitude, but loses its skill as stronger nonlinearity takes place in the model (Lutsko et al. 2015; Gritsun et al. 2008) and often for nonlinear observables like the variance.

Finally, the systematic approach we develop in this paper shows potential to be applied to more realistic climate models. Also, passive tracer advected by the geophysical turbulent flow contains a number of attractive features and is worth investigating under this framework. It is worthwhile to pursue similar analysis and application of the reduced-order models about turbulent tracer advection in the geophysical flow.

Acknowledgments. This research of the Andrew Majda is partially supported by the Office of Naval Research through MURI N00014-16-1-2161 and DARPA through W911NF-15-1-0636. Di Qi is supported as a graduate research assistant on these grant.

APPENDIX A

Detailed explicit formulations about the two-layer QG flow

Here we list the explicit formulations about the statistical dynamics (7) of the two-layer QG equations described in (4)

$$\frac{d\mathbf{p_k}}{dt} = B_{\mathbf{k}}\left(\mathbf{p_k},\mathbf{p_k}\right) + \left(\mathscr{L}_{\mathbf{k}} - \mathscr{D}_{\mathbf{k}}\right)\mathbf{p_k} + \mathscr{F}_{\mathbf{k}}, \quad \mathbf{p_k} = \left(p_{\psi,\mathbf{k}}, p_{\tau,\mathbf{k}}\right)^T. \tag{A1}$$

The nonlinear interactions include the energy conserving quadratic forms between barotropic and baroclinic modes

$$B_{\mathbf{k}}\left(\mathbf{p_k},\mathbf{p_k}\right) = \begin{bmatrix} \sum_{\mathbf{m}+\mathbf{n}=\mathbf{k}} \frac{\mathbf{m}^{\perp}\cdot\mathbf{n}}{|\mathbf{k}|}\left(\frac{|\mathbf{n}|}{|\mathbf{m}|}p_{\psi,\mathbf{m}}p_{\psi,\mathbf{n}} + \sqrt{\frac{|\mathbf{n}|^2+k_d^2}{|\mathbf{m}|^2+k_d^2}}p_{\tau,\mathbf{m}}p_{\tau,\mathbf{n}}\right) \\ \sum_{\mathbf{m}+\mathbf{n}=\mathbf{k}} \frac{\mathbf{m}^{\perp}\cdot\mathbf{n}}{\sqrt{|\mathbf{k}|^2+k_d^2}}\left(\frac{\sqrt{|\mathbf{n}|^2+k_d^2}}{|\mathbf{m}|}p_{\psi,\mathbf{m}}p_{\tau,\mathbf{n}} + \frac{|\mathbf{n}|}{\sqrt{|\mathbf{m}|^2+k_d^2}}p_{\tau,\mathbf{m}}p_{\psi,\mathbf{n}}\right) \end{bmatrix}; \tag{A2}$$

and the linear operators are decomposed into the non-symmetric part $\mathscr{L}_{\mathbf{k}}$ and dissipation part $\mathscr{D}_{\mathbf{k}}$ for Ekman friction (we neglect the additional terms for hyperviscosity), together with the forcing

$\mathscr{F}_{\mathbf{k}}$ combining deterministic component and stochastic component

$$\mathscr{L}_{\mathbf{k}}=\begin{bmatrix} \frac{ik_x\beta}{|\mathbf{k}|^2} & -\frac{ik_xU}{\sqrt{1+(k_d/|\mathbf{k}|)^2}} \\ -ik_xU\frac{1-(k_d/|\mathbf{k}|)^2}{\sqrt{1+(k_d/|\mathbf{k}|)^2}} & \frac{ik_x\beta}{|\mathbf{k}|^2+k_d^2} \end{bmatrix},\ \mathscr{D}_{\mathbf{k}}=\frac{\kappa}{2}\begin{bmatrix} -1 & \frac{1}{\sqrt{1+(k_d/|\mathbf{k}|)^2}} \\ \frac{1}{\sqrt{1+(k_d/|\mathbf{k}|)^2}} & -\frac{1}{1+(k_d/|\mathbf{k}|)^2} \end{bmatrix},\ \mathscr{F}_{\mathbf{k}}=\begin{bmatrix} \frac{f_{\psi,\mathbf{k}}}{|\mathbf{k}|}+\frac{\sigma_{\psi,\mathbf{k}}\dot{W}_{\psi,\mathbf{k}}}{|\mathbf{k}|} \\ \frac{f_{\tau,\mathbf{k}}}{\sqrt{|\mathbf{k}|^2+k_d^2}}+\frac{\sigma_{\tau,\mathbf{k}}\dot{W}_{\tau,\mathbf{k}}}{\sqrt{|\mathbf{k}|^2+k_d^2}} \end{bmatrix}. \tag{A3}$$

The statistical dynamical equations concern about the variances in both barotropic and baroclinic mode, $\overline{|p_{\psi,\mathbf{k}}|^2}$ and $\overline{|p_{\tau,\mathbf{k}}|^2}$, together with the covariance between the modes within the same wavenumber, $\overline{p^*_{\psi,\mathbf{k}}p_{\tau,\mathbf{k}}}$,

$$\begin{aligned}
&\frac{d}{dt}\overline{|p_{\psi,\mathbf{k}}|^2}+2\mathfrak{Re}\frac{ik_x|\mathbf{k}|U}{\sqrt{|\mathbf{k}|^2+k_d^2}}\overline{p^*_{\psi,\mathbf{k}}p_{\tau,\mathbf{k}}}+Q_{\psi,\mathbf{k}}=\kappa\left(-\overline{|p_{\psi,\mathbf{k}}|^2}+\frac{|\mathbf{k}|}{\sqrt{|\mathbf{k}|^2+k_d^2}}\mathfrak{Re}\overline{p^*_{\psi,\mathbf{k}}p_{\tau,\mathbf{k}}}\right)+\frac{\sigma^2_{\psi,\mathbf{k}}}{|\mathbf{k}|^2},\\
&\frac{d}{dt}\overline{|p_{\tau,\mathbf{k}}|^2}+2\mathfrak{Re}\frac{ik_xU}{\sqrt{|\mathbf{k}|^2+k_d^2}}\frac{|\mathbf{k}|^2-k_d^2}{|\mathbf{k}|}\overline{p_{\psi,\mathbf{k}}p^*_{\tau,\mathbf{k}}}+Q_{\tau,\mathbf{k}}=\kappa\left(\frac{|\mathbf{k}|}{\sqrt{|\mathbf{k}|^2+k_d^2}}\mathfrak{Re}\overline{p_{\psi,\mathbf{k}}p^*_{\tau,\mathbf{k}}}-\frac{|\mathbf{k}|^2}{|\mathbf{k}|^2+k_d^2}\overline{|p_{\tau,\mathbf{k}}|^2}\right)+\frac{\sigma^2_{\tau,\mathbf{k}}}{|\mathbf{k}|^2+k_d^2},\\
&\frac{d}{dt}\overline{p^*_{\psi,\mathbf{k}}p_{\tau,\mathbf{k}}}+\frac{ik_x\beta}{|\mathbf{k}|^2}\overline{p^*_{\psi,\mathbf{k}}p_{\tau,\mathbf{k}}}-\frac{ik_xU}{\sqrt{|\mathbf{k}|^2+k_d^2}}\overline{|p_{\tau,\mathbf{k}}|^2}+Q_{c,\mathbf{k}}=-\frac{\kappa}{2}\left(\overline{p^*_{\psi,\mathbf{k}}p_{\tau,\mathbf{k}}}-\frac{|\mathbf{k}|}{\sqrt{|\mathbf{k}|^2+k_d^2}}\overline{|p_{\tau,\mathbf{k}}|^2}\right)\\
&\quad-\frac{ik_x\beta}{|\mathbf{k}|^2+k_d^2}\overline{p^*_{\psi,\mathbf{k}}p_{\tau,\mathbf{k}}}+\frac{ik_xU}{\sqrt{|\mathbf{k}|^2+k_d^2}}\frac{|\mathbf{k}|^2-k_d^2}{|\mathbf{k}|}\overline{|p_{\psi,\mathbf{k}}|^2}\quad+\frac{\kappa}{2}\left(-\frac{|\mathbf{k}|^2}{|\mathbf{k}|^2+k_d^2}\overline{p^*_{\psi,\mathbf{k}}\psi_{\tau,\mathbf{k}}}+\frac{|\mathbf{k}|}{\sqrt{|\mathbf{k}|^2+k_d^2}}\overline{|p_{\psi,\mathbf{k}}|^2}\right).
\end{aligned} \tag{A4}$$

where the first terms on the left hand sides represent the linear interactions as $(\mathscr{L}_{\mathbf{k}}-\mathscr{D}_{\mathbf{k}})R_{\mathbf{k}}$ in (7); $Q_{\psi,\mathbf{k}},Q_{\tau,\mathbf{k}},Q_{c,\mathbf{k}}$ are from higher-order moments as well as the terms due to the mean-covariance interactions. Importantly, these nonlinear flux terms Q_F represent the nonlinear interactions between different wavenumbers due to the advection term. The explicit form will include third-order moments so that

$$Q_{\psi,\mathbf{k}}=\sum_{\mathbf{m}+\mathbf{n}=\mathbf{k}}\frac{\mathbf{m}^{\perp}\cdot\mathbf{n}}{|\mathbf{k}|}\left(\frac{|\mathbf{n}|}{|\mathbf{m}|}\overline{p_{\psi,\mathbf{k}}^{*}p_{\psi,\mathbf{m}}p_{\psi,\mathbf{n}}}+\sqrt{\frac{|\mathbf{n}|^{2}+k_{d}^{2}}{|\mathbf{m}|^{2}+k_{d}^{2}}}\overline{p_{\psi,\mathbf{k}}^{*}p_{\tau,\mathbf{m}}p_{\tau,\mathbf{n}}}\right),$$

$$Q_{\tau,\mathbf{k}}=\sum_{\mathbf{m}+\mathbf{n}=\mathbf{k}}\frac{\mathbf{m}^{\perp}\cdot\mathbf{n}}{\sqrt{|\mathbf{k}|^{2}+k_{d}^{2}}}\left(\frac{\sqrt{|\mathbf{n}|^{2}+k_{d}^{2}}}{|\mathbf{m}|}\overline{p_{\tau,\mathbf{k}}^{*}p_{\psi,\mathbf{m}}p_{\tau,\mathbf{n}}}+\frac{|\mathbf{n}|}{\sqrt{|\mathbf{m}|^{2}+k_{d}^{2}}}\overline{p_{\tau,\mathbf{k}}^{*}p_{\tau,\mathbf{m}}p_{\psi,\mathbf{n}}}\right),$$

$$\begin{aligned}Q_{c,\mathbf{k}}=&\sum_{\mathbf{m}+\mathbf{n}=\mathbf{k}}\frac{\mathbf{m}^{\perp}\cdot\mathbf{n}}{|\mathbf{k}|}\left(\frac{|\mathbf{n}|}{|\mathbf{m}|}\overline{p_{\tau,\mathbf{k}}p_{\psi,\mathbf{m}}^{*}p_{\psi,\mathbf{n}}^{*}}+\sqrt{\frac{|\mathbf{n}|^{2}+k_{d}^{2}}{|\mathbf{m}|^{2}+k_{d}^{2}}}\overline{p_{\tau,\mathbf{k}}p_{\tau,\mathbf{m}}^{*}p_{\tau,\mathbf{n}}^{*}}\right)\\&+\sum_{\mathbf{m}+\mathbf{n}=\mathbf{k}}\frac{\mathbf{m}^{\perp}\cdot\mathbf{n}}{\sqrt{|\mathbf{k}|^{2}+k_{d}^{2}}}\left(\frac{\sqrt{|\mathbf{n}|^{2}+k_{d}^{2}}}{|\mathbf{m}|}\overline{p_{\psi,\mathbf{k}}^{*}p_{\psi,\mathbf{m}}p_{\tau,\mathbf{n}}}+\frac{|\mathbf{n}|}{\sqrt{|\mathbf{m}|^{2}+k_{d}^{2}}}\overline{p_{\psi,\mathbf{k}}^{*}p_{\tau,\mathbf{m}}p_{\psi,\mathbf{n}}}\right).\end{aligned}$$

Note that mean-covariance interactions (like $\bar{p}_{\mathbf{k}}\overline{p_{\mathbf{m}}^{\prime}p_{\mathbf{n}}^{\prime *}}$) and third-order moments (like $\overline{p_{\mathbf{k}}^{\prime}p_{\mathbf{m}}^{\prime}p_{\mathbf{n}}^{\prime *}}$) with triad modes $\mathbf{m}+\mathbf{n}=\mathbf{k}$ are both included in the nonlinear flux representing the nonlinear energy transfer between small and large scales.

Finally we give the explicit form of the total statistical energy equation in (10) as

$$\begin{aligned}\frac{d}{dt}E+k_{d}^{2}U\sum_{1\leq|\mathbf{k}|\leq N}ik_{x}\overline{\psi_{\mathbf{k}}^{*}\tau_{\mathbf{k}}}=&-\kappa E+\frac{\kappa}{2}\sum_{1\leq|\mathbf{k}|\leq N}\left(k_{d}^{2}\overline{|\tau_{\mathbf{k}}|^{2}}+2|\mathbf{k}|^{2}\overline{\psi_{\mathbf{k}}^{*}\tau_{\mathbf{k}}}\right)\\&\sum_{1\leq|\mathbf{k}|\leq N}-\nu|\mathbf{k}|^{2s}\left(\overline{|p_{\psi,\mathbf{k}}|^{2}}+\overline{|p_{\tau,\mathbf{k}}|^{2}}\right)+\frac{1}{2}\left(\frac{\sigma_{\psi,\mathbf{k}}^{2}}{|\mathbf{k}|^{2}}+\frac{\sigma_{\tau,\mathbf{k}}^{2}}{|\mathbf{k}|^{2}+k_{d}^{2}}\right),\end{aligned}\tag{A5}$$

where $E=\frac{1}{2}\sum_{1\leq|\mathbf{k}|\leq N}\left(\overline{|p_{\psi,\mathbf{k}}|^{2}}+\overline{|p_{\tau,\mathbf{k}}|^{2}}\right)$ defines the total total statistical energy. The second term on the left hand side is due to the heat flux from baroclinic instability, and the terms on the right hand side are from dissipation as well as the total external forcing effects in the last term.

APPENDIX B

Linear response theory for stochastic perturbation

We derive the detailed formulas for the linear response operators with stochastic perturbation in this part (the deterministic perturbation case can be derived in a similar way as in Majda and Wang (2010)). In this case, we focus on the system perturbation induced by a stochastic noise term. In general we consider the perturbed system

$$\frac{d\mathbf{u}}{dt} = \mathbf{F}(\mathbf{u}) + \left(\sigma_0 + \sqrt{\delta}\sigma\right)\dot{\mathbf{W}}. \tag{B1}$$

The linear response calculation for the stochastic perturbation in (B1) assumes that the perturbed distribution has the decomposition

$$p^{\delta} = p_{\mathrm{eq}} + \delta p + O\left(\delta^2\right).$$

In the leading order *Fokker-Planck equation* for the perturbation in probability density δp we have the dynamics

$$\begin{aligned}\frac{\partial \delta p}{\partial t} = & -\nabla\cdot(\delta p\mathbf{F}) + \frac{1}{2}\nabla\nabla\cdot\left(\sigma_0\sigma_0^T\sqrt{\delta}p\right)\\ & + \frac{1}{2}\nabla\nabla\cdot\left[\left(\sigma_0\sqrt{\delta}\sigma^T + \sqrt{\delta}\sigma\sigma_0^T + \delta\sigma\sigma^T\right)p_{\mathrm{eq}}\right].\end{aligned}$$

Here we assume the unperturbed system is deterministic $\sigma_0 \equiv 0$ (that is consistent with the two-layer model we are using in most applications in the main text). This is why we assume the perturbation is in the order $O\left(\sqrt{\delta}\right)$, and the Fokker-Planck operator corresponding to the stochastic perturbation to the deterministic unperturbed system becomes

$$\mathscr{L}_{\sigma}p = \frac{1}{2}\nabla\nabla\cdot\left[\sigma\sigma^T p\right].$$

Therefore we find the *linear response operator corresponding to the stochastic perturbation to the deterministic unperturbed system*

$$\mathscr{R}_{\sigma,A} = \left\langle A\left(\mathbf{u}(t)\right)B_{\sigma}\left(\mathbf{u}(0)\right)\right\rangle,\ B_{\sigma}\left(\mathbf{u}\right) = \frac{\mathscr{L}_{\sigma}p_{\mathrm{eq}}}{p_{\mathrm{eq}}}. \tag{B2}$$

In the two-layer system, the exact form of unperturbed equilibrium distribution p_{eq} is still unavailable and may always include non-Gaussian statistics. However, it is useful to make the quasi-Gaussian approximation about each spectral mode and assume independence between modes with different wavenumbers (Majda et al. 2005; Abramov and Majda 2012)

$$p_{\mathrm{eq}} \sim \prod \exp\left(-\frac{1}{2}\mathbf{p_k}^* R_{\mathbf{k}}^{-1}\mathbf{p_k}\right),\ \mathbf{p_k} = \left(p_{\psi,\mathbf{k}}, p_{\tau,\mathbf{k}}\right)^T. \tag{B3}$$

Above $\mathbf{p_k}$ is the scaled state variable including the barotropic and baroclinic mode in the same wavenumber as in the main text. The Gaussian approximation in (B3) is reasonable, and the joint-distributions in Figure 7 in main text also show that the state variables in the spectral domain are correlated majorly between barotropic and baroclinic mode with the same wavenumber and decoupled in different wavenumber mode. Substitution of (B3) into the linear response formula (B2) will give us the explicit formulation about the linear response operator. First note that using $A(\mathbf{p}) = \mathbf{p}$, the responses to the first-order moment are vanishing to the stochastic perturbations consistent with the equation predictions. Then we need to focus on the linear responses in the second order moments $A(\mathbf{p}) = \mathbf{p}^2$. Second derivatives of the equilibrium measure p_{eq} are required, and the forth moments are needed for calculating the linear response operators. Further in this case, we assume the contribution from the modes with different wavenumbers are negligible, $\left\langle p_{\mathbf{k}}^2(t)\, p_{\mathbf{l}}^2(0)\right\rangle \sim 0$. Thus we get the approximation for the linear response operators in the barotropic $\mathscr{R}_{\sigma,\psi,\mathbf{k}}$ and baroclinic $\mathscr{R}_{\sigma,\psi,\mathbf{k}}$ mode in each wavenumber $\mathbf{k}$ due to a barotropic perturbation with white noise variance $\delta\sigma_{\psi,\mathbf{k}}^2$

$$\begin{aligned}
\mathscr{R}_{\sigma,\psi,\mathbf{k}} &= \frac{\delta\sigma_{\sigma,\mathbf{k}}^2}{2}\left[-a_{\mathbf{k}} r_{\psi,\mathbf{k}} + \left(a_{\mathbf{k}}^2 \overline{\left|p_{\psi,\mathbf{k}}\right|^2(t)\left|p_{\psi,\mathbf{k}}\right|^2(0)} + |c_{\mathbf{k}}|^2\, \overline{\left|p_{\psi,\mathbf{k}}\right|^2(t)\left|p_{\tau,\mathbf{k}}\right|^2(0)} + 2\mathfrak{Re}c_{\mathbf{k}}\overline{\left|p_{\psi,\mathbf{k}}\right|^2(t)\, p_{\psi,\mathbf{k}}^* p_{\tau,\mathbf{k}}(0)}\right)\right],\\
\mathscr{R}_{\sigma,\tau,\mathbf{k}} &= \frac{\delta\sigma_{\sigma,\mathbf{k}}^2}{2}\left[-a_{\mathbf{k}} r_{\tau,\mathbf{k}} + \left(a_{\mathbf{k}}^2 \overline{\left|p_{\tau,\mathbf{k}}\right|^2(t)\left|p_{\psi,\mathbf{k}}\right|^2(0)} + |c_{\mathbf{k}}|^2\, \overline{\left|p_{\tau,\mathbf{k}}\right|^2(t)\left|p_{\tau,\mathbf{k}}\right|^2(0)} + 2\mathfrak{Re}c_{\mathbf{k}}\overline{\left|p_{\tau,\mathbf{k}}\right|^2(t)\, p_{\psi,\mathbf{k}}^* p_{\tau,\mathbf{k}}(0)}\right)\right].
\end{aligned} \tag{B4}$$

with entries of the inverse of covariance matrix assumed as

$$R_{\mathbf{k}}^{-1}=\begin{bmatrix} a_{\mathbf{k}} & c_{\mathbf{k}} \\ c_{\mathbf{k}}^{*} & b_{\mathbf{k}} \end{bmatrix}.$$

The lagged forth-order moments in (B4) can be achieved through averaging along a trajectory in statistical steady state due to the ergodicity of the two-layer model.

In real simulations, the true linear response operators can be calculated directly from (B4), while for the reduced-order models the kicked response strategy (Majda et al. 2005; Majda and Qi 2016) is adopted. We summarize the strategies in achieving the linear response operators in both true system and the reduced-order models as follows:

- *True linear response operator from equilibrium statistics*: The true linear response operator is calculated through the formula derived in (B4). The lagged forth-order moments are calculated exactly by averaging over a long simulation trajectory in statistical steady state;

- *Imperfect model response operator from kicked response of the variance*: kicked response for the second moments is applied to get the imperfect model response operator. In the initial value, the variance is kicked from equilibrium value by a small amplitude, $R_{\mathbf{k},\mathrm{init}}=R_{\mathbf{k},\mathrm{eq}}+\delta R_{\mathbf{k}}$. Then the unperturbed system is used with this perturbed initial variance. The linear response operator can be approximated from the model response in the second-order moments.

References

Abramov, R. V., and A. J. Majda, 2012: Low-frequency climate response of quasigeostrophic wind-driven ocean circulation. *Journal of Physical Oceanography*, **42 (2)**, 243–260.

Deser, C., and M. L. Blackmon, 1993: Surface climate variations over the north atlantic ocean during winter: 1900-1989. *Journal of Climate*, **6 (9)**, 1743–1753.

Gettelman, A., J. Kay, and K. Shell, 2012: The evolution of climate sensitivity and climate feedbacks in the community atmosphere model. *Journal of Climate*, **25 (5)**, 1453–1469.

Gritsun, A., and G. Branstator, 2007: Climate response using a three-dimensional operator based on the fluctuation-dissipation theorem. *Journal of the atmospheric sciences*, **64 (7)**, 2558–2575.

Gritsun, A., G. Branstator, and A. Majda, 2008: Climate response of linear and quadratic functionals using the fluctuation-dissipation theorem. *Journal of the Atmospheric Sciences*, **65 (9)**, 2824–2841.

Grooms, I., and A. J. Majda, 2013: Efficient stochastic superparameterization for geophysical turbulence. *Proceedings of the National Academy of Sciences*, **110 (12)**, 4464–4469.

Harlim, J., and A. J. Majda, 2010: Filtering turbulent sparsely observed geophysical flows. *Monthly Weather Review*, **138 (4)**, 1050–1083.

Kullback, S., and R. A. Leibler, 1951: On information and sufficiency. *The annals of mathematical statistics*, **22 (1)**, 79–86.

Kushnir, Y., 1994: Interdecadal variations in north atlantic sea surface temperature and associated atmospheric conditions. *Journal of Climate*, **7 (1)**, 141–157.

Leith, C., 1975: Climate response and fluctuation dissipation. *Journal of the Atmospheric Sciences*, **32 (10)**, 2022–2026.

Lutsko, N. J., I. M. Held, and P. Zurita-Gotor, 2015: Applying the fluctuation–dissipation theorem to a two-layer model of quasigeostrophic turbulence. *Journal of the Atmospheric Sciences*, **72 (8)**, 3161–3177.

Majda, A., 2016: *An introduction to turbulent dynamical systems for complex systems*. 1st ed., Springer International Publishing.

Majda, A., R. V. Abramov, and M. J. Grote, 2005: *Information theory and stochastics for multiscale nonlinear systems*, Vol. 25. American Mathematical Soc.

Majda, A., and X. Wang, 2006: *Nonlinear dynamics and statistical theories for basic geophysical flows*. Cambridge University Press.

Majda, A., and X. Wang, 2010: Linear response theory for statistical ensembles in complex systems with time-periodic forcing. *Communications in Mathematical Sciences*, **8 (1)**, 145–172.

Majda, A. J., 2015: Statistical energy conservation principle for inhomogeneous turbulent dynamical systems. *Proceedings of the National Academy of Sciences*, **112 (29)**, 8937–8941.

Majda, A. J., and B. Gershgorin, 2011: Link between statistical equilibrium fidelity and forecasting skill for complex systems with model error. *Proceedings of the National Academy of Sciences*, **108 (31)**, 12 599–12 604.

Majda, A. J., B. Gershgorin, and Y. Yuan, 2010: Low-frequency climate response and fluctuation-dissipation theorems: theory and practice. *Journal of the Atmospheric Sciences*, **67 (4)**, 1186–1201.

Majda, A. J., and D. Qi, 2016: Improving prediction skill of imperfect turbulent models through statistical response and information theory. *Journal of Nonlinear Science*, **26 (1)**, 233–285.

Panetta, R. L., 1993: Zonal jets in wide baroclinically unstable regions: Persistence and scale selection. *Journal of the atmospheric sciences*, **50 (14)**, 2073–2106.

Pavan, V., and I. M. Held, 1996: The diffusive approximation for eddy fluxes in baroclinically unstable jets. *Journal of the atmospheric sciences*, **53 (9)**, 1262–1272.

Qi, D., and A. J. Majda, 2016: Low-dimensional reduced-order models for statistical response and uncertainty quantification: barotropic turbulence with topography. *submitted to Physica D: Nonlinear Phenomena*.

Salmon, R., 1998: *Lectures on geophysical fluid dynamics*. Oxford University Press.

Sapsis, T. P., and A. J. Majda, 2013a: Statistically accurate low-order models for uncertainty quantification in turbulent dynamical systems. *Proceedings of the National Academy of Sciences*, **110 (34)**, 13 705–13 710.

Sapsis, T. P., and A. J. Majda, 2013b: A statistically accurate modified quasilinear gaussian closure for uncertainty quantification in turbulent dynamical systems. *Physica D: Nonlinear Phenomena*, **252**, 34–45.

Thompson, A. F., and W. R. Young, 2007: Two-layer baroclinic eddy heat fluxes: Zonal flows and energy balance. *Journal of the Atmospheric Sciences*, **64 (9)**, 3214–3231.

Treguier, A. M., and B. L. Hua, 1987: Oceanic quasi-geostrophic turbulence forced by stochastic wind fluctuations. *Journal of physical oceanography*, **17 (3)**, 397–411.

Vallis, G. K., 2006: *Atmospheric and oceanic fluid dynamics: fundamentals and large-scale circulation*. Cambridge University Press.

Zurita-Gotor, P., J. Blanco-Fuentes, and E. P. Gerber, 2014: The impact of baroclinic eddy feedback on the persistence of jet variability in the two-layer model. *Journal of the Atmospheric Sciences*, **71 (1)**, 410–429.

LIST OF TABLES

TABLE 1. Model parameters for ocean and atmosphere dynamical regimes in high latitude. N is the model resolution, β, k_d are the rotation parameter and the deformation frequency, U is the background mean shear flow, κ is the Ekman drag in the bottom layer, and the hyperviscosity is measured by the operator $-\nu\nabla^{2s}$. The last three columns display the unstable waveband from linear analysis. $(k_{\min}, k_{\max})$ shows the range of unstable wavenumbers; $\sigma_{\max}$ is the largest linear growth rate; and $(k_x, k_y)_{\max}$ is the position of the mode with maximum growth rate.

regime	N	β	k_d	U	κ	ν	s	$(k_{\min}, k_{\max})$	$\sigma_{\max}$	$(k_x, k_y)_{\max}$
ocean regime, high lat.	256	10	10	1	9	1.2×10^{-15}	4	$(2.25, 14.61)$	0.411	(4, 0)
atmosphere regime, high lat.	256	1	4	0.2	0.2	5×10^{-15}	4	$(1.58, 6.78)$	0.099	(2, 0)

TABLE 2. Model parameters for ocean and atmosphere dynamical regimes in low/mid latitude. N is the model resolution, β, k_d are the rotation parameter and the deformation frequency, U is the background mean shear flow, κ is the Ekman drag in the bottom layer, and the hyperviscosity is measured by the operator $-\nu\nabla^{2s}$. The last three columns display the unstable waveband from linear analysis. $(k_{\min}, k_{\max})$ shows the range of unstable wavenumbers; $\sigma_{\max}$ is the largest linear growth rate; and $(k_x, k_y)_{\max}$ is the position of the mode with maximum growth rate.

regime	N	β	k_d	U	κ	ν	s	$(k_{\min}, k_{\max})$	$\sigma_{\max}$	$(k_x, k_y)_{\max}$
ocean regime, low/mid lat.	256	100	10	1	1	1.2×10^{-15}	4	$(7.14, 15.63)$	0.104	(2, 8)
atmosphere regime, low/mid lat.	256	2.5	4	0.2	0.05	5×10^{-15}	4	$(2.51, 7.06)$	0.053	(3, 0)

LIST OF FIGURES

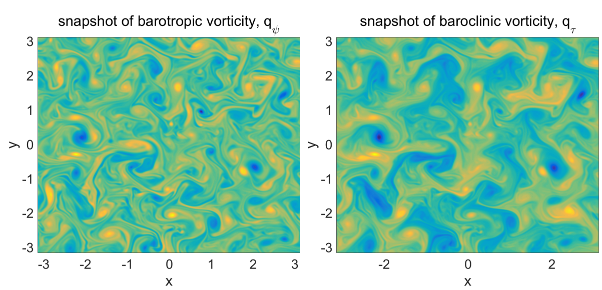

(a) snapshots of relative vorticity

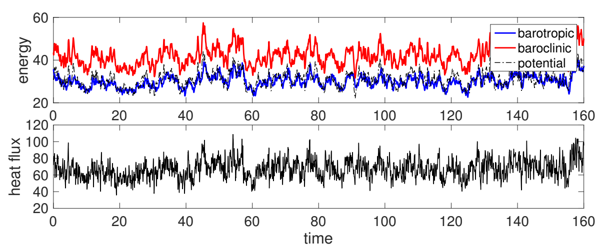

(b) time-series of energy and heat flux

FIG. 1. Snapshots of the unperturbed system in high-latitude ocean regime with no external forcing terms. The barotropic and baroclinic vorticity in steady state are plotted. Time-series of energy in barotropic and baroclinic modes, as well as potential energy, are compared with the heat flux.

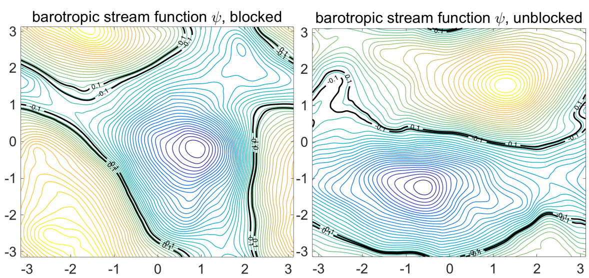

(a) snapshots of stream function

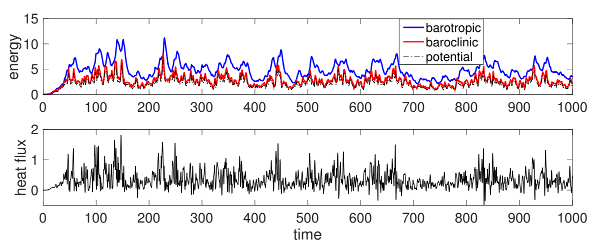

(b) time-series of energy and heat flux

FIG. 2. Snapshots of the unperturbed system in high-latitude atmosphere regime with no external forcing terms. The barotropic stream functions in blocked and unblocked state are plotted. The time-series for barotropic, baroclinic, and potential energy are compared with the heat flux in the following part.

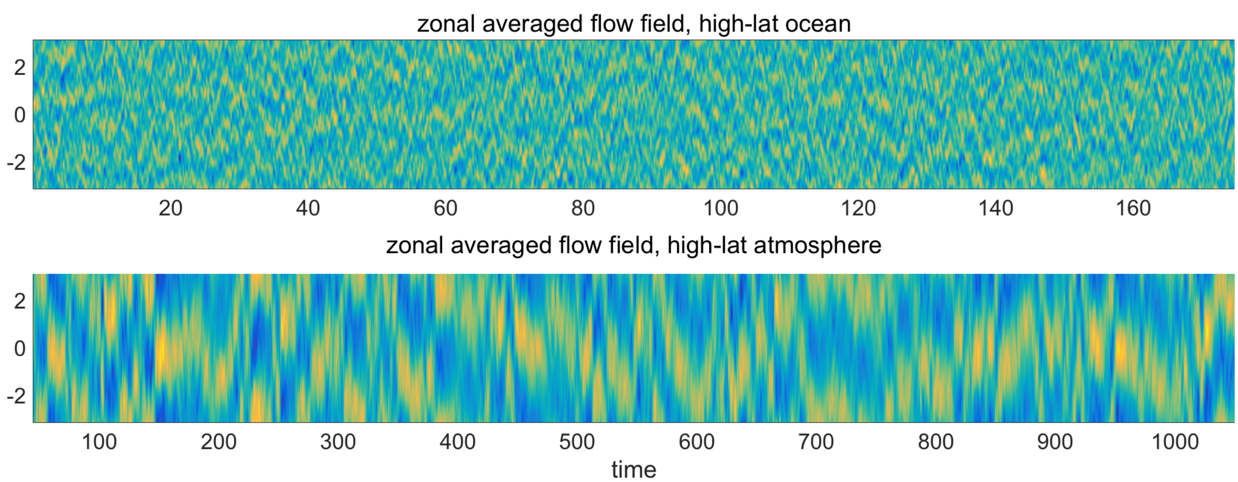

FIG. 3. Time-series of zonal mean flow in high-latitude regime.

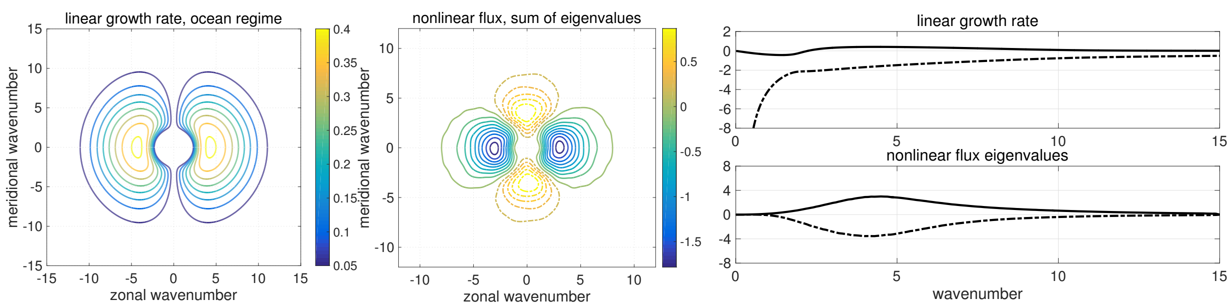

(a) high-latitude ocean regime

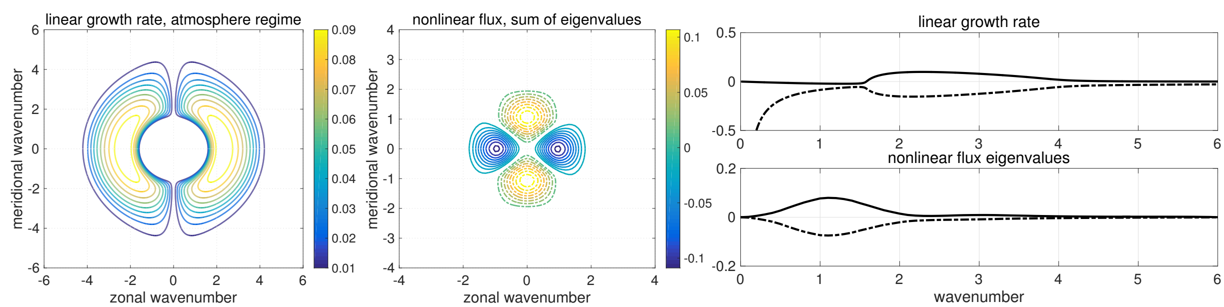

(b) high-latitude atmosphere regime

FIG. 4. Stability from linear analysis and nonlinear flux in ocean (upper) and atmosphere (lower) regime using parameters in Table 1. The growth rate from linear analysis including Ekman damping effect, and the eigenvalues of the nonlinear flux $\mathrm{tr}Q_{F,\mathbf{k}}$ in each wavenumber combining barotropic and baroclinic mode are displayed in the two-dimensional spectral domain. The last column shows the radial averaged growth rate and nonlinear flux eigenvalues in positive and negative components.

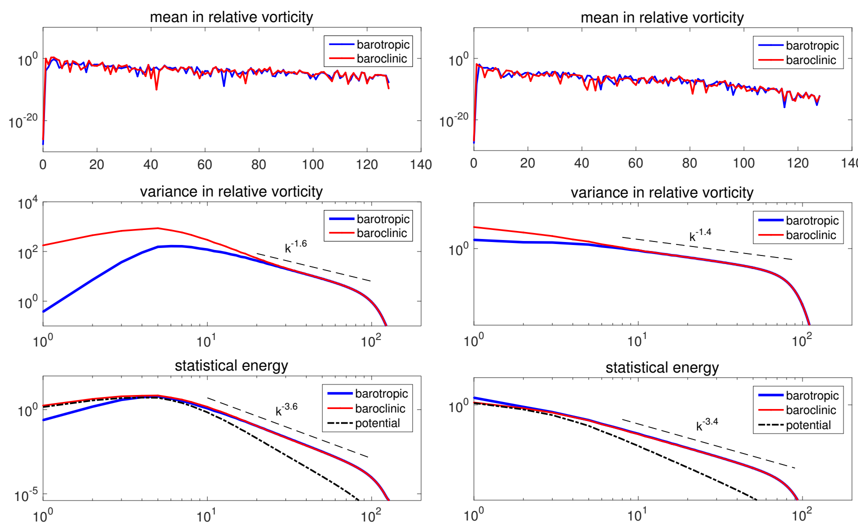

(a) ocean regime (b) atmosphere regime

FIG. 5. Time-averaged statistics (in radial average) in mean and second-order moments in high-latitude regime. The first row compares the statistical mean states. The following two rows show the variances, $\overline{|q_{\psi,k}|^2}$, $\overline{|q_{\tau,k}|^2}$, and statistical energy, $|k|^2\overline{|\psi_k|^2}$, $\left(|k|^2+k_d^2\right)\overline{|\tau_k|^2}$, in barotropic and baroclinic modes, as well as the potential energy $k_d^2\overline{|\tau_k|^2}$.

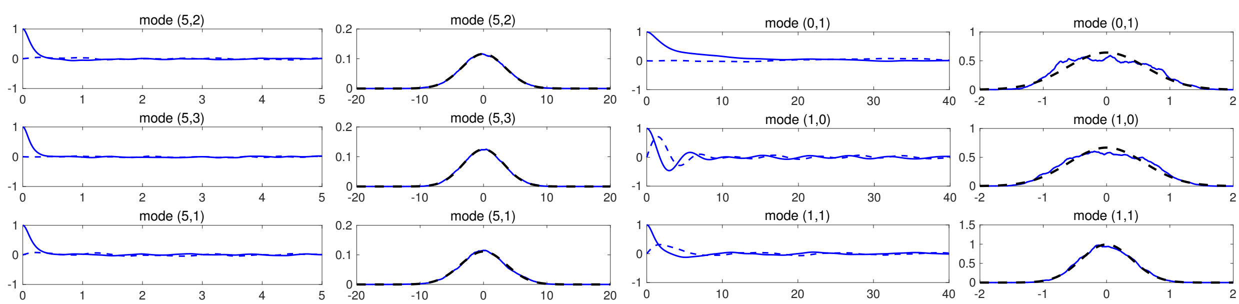

(a) ocean regime (b) atmosphere regime

FIG. 6. Autocorrelation functions and the probability distribution functions in high-latitude ocean (left) and atmosphere (right) regime. The first three most energetic baroclinic modes are displayed. In the autocorrelations, the solid lines show the real part while the dashed lines are the imaginary part of the functions. In the pdfs, the corresponding Gaussian distributions with the same variance are also plotted in dashed black lines.

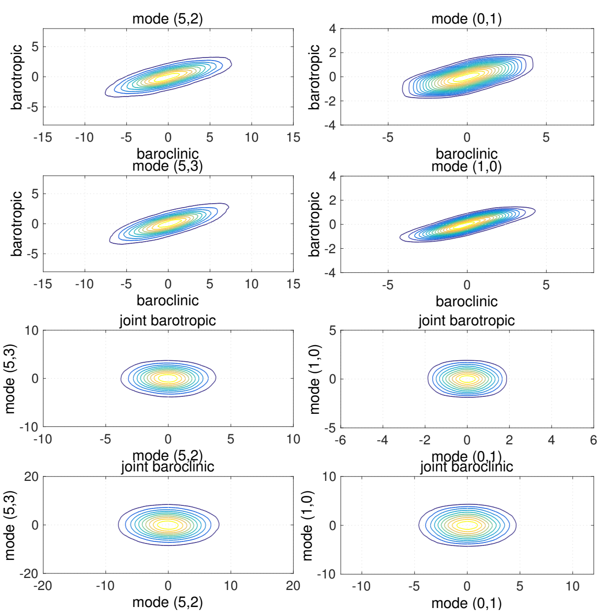

(a) ocean (b) atmosphere

FIG. 7. Joint-distributions in the most energetic modes in the ocean (mode $(5,2)$ and $(5,3)$) and atmosphere (mode $(1,0)$ and $(0,1)$) regime. The first two rows show the joint-distribution in barotropic and baroclinic modes in the principal modes. And the second parts show the joint-distributions between barotropic and baroclinic modes with different wavenumbers.

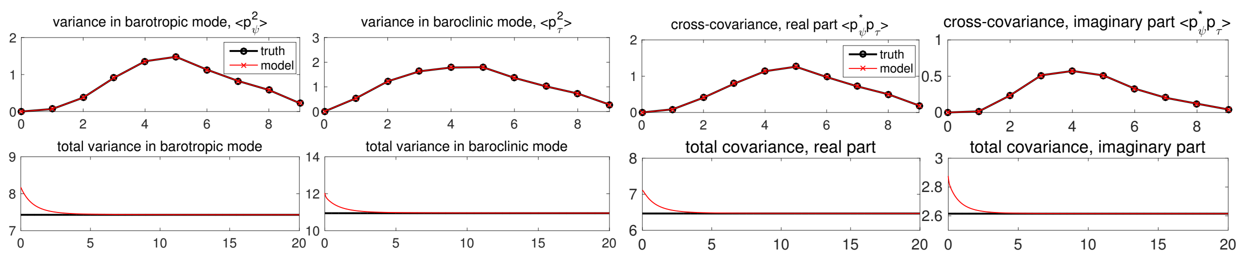

(a) variances in equilibrium (b) cross-covariances in equilibrium

FIG. 8. Equilibrium consistency for the reduced-order models. The first row is the unperturbed equilibrium spectra for the variances and cross-covariances between barotropic and baroclinic mode in radial averaged mode. And the time series of the total variances and covariances are followed. The true model results are shown in black, while the reduced-order model results are in red.

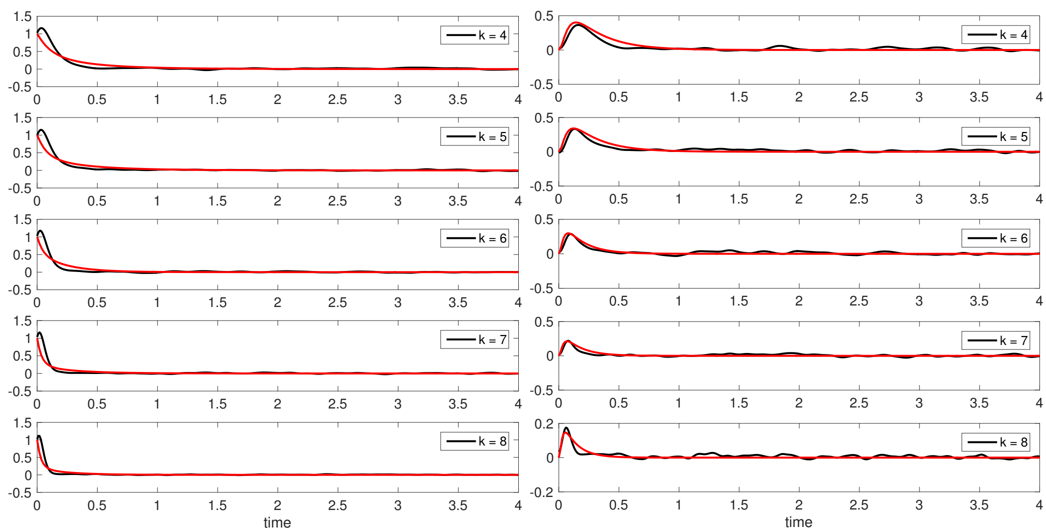

(a) barotropic response operator (b) baroclinic response operator

FIG. 9. Linear response operator (radial averaged) in high-latitude ocean regime in barotropic and baroclinic mode when the barotropic mode is randomly perturbed. The black lines are the truth from the formula (B4) using equilibrium statistics, and the red lines are the kicked-responses from the imperfect model.

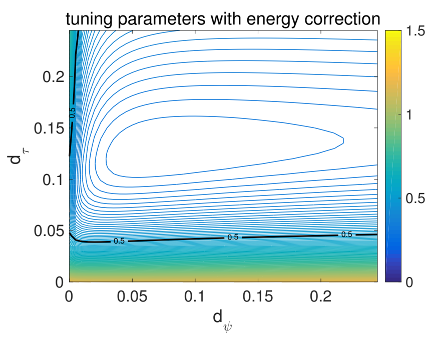

(a) tuning with energy scaling

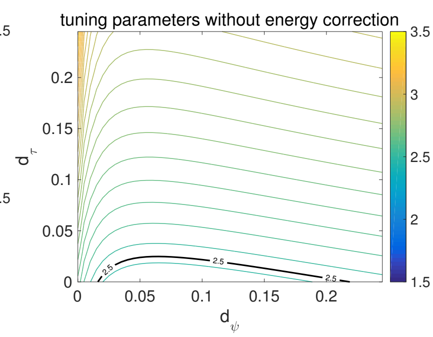

(b) tuning without energy scaling

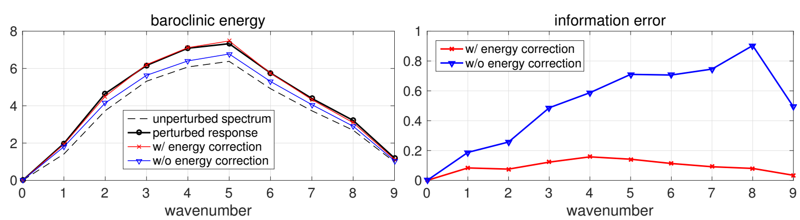

(c) prediction and info. errors

FIG. 10. Tuning imperfect model parameters in the training phase. The information errors with varying model parameters, $d_M = \left(d_\psi, d_\tau\right)$, are plotted for stochastic barotropic perturbation case. The errors using total energy as scalar factor from the statistical equation and method without the scaling factor are compared. The prediction skill and information error with and without using the total energy correction are compared in the last row for a typical test case of perturbing the barotropic mode.

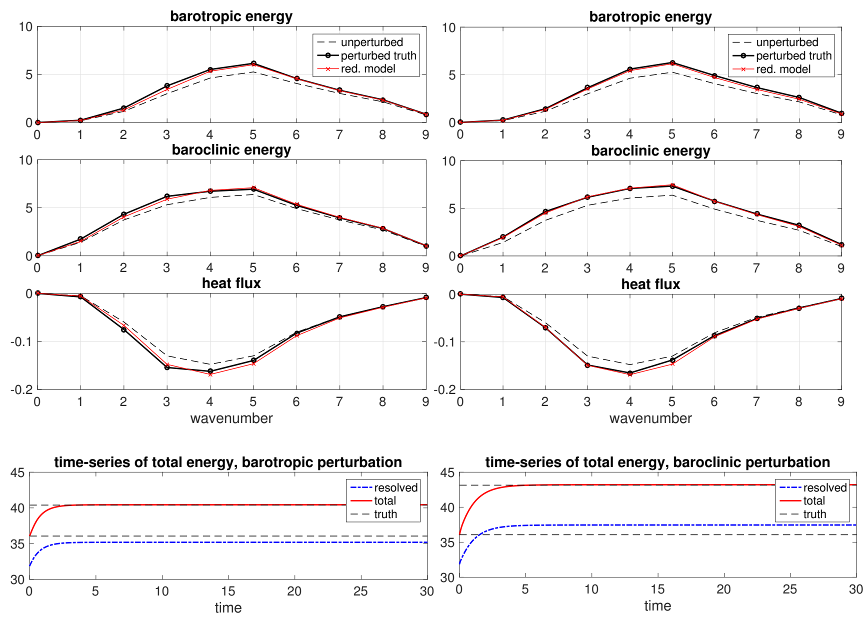

(a) barotropic perturbation (b) baroclinic perturbation

FIG. 11. Reduced-order model predictions to stochastic perturbations with amplitude $\delta\sigma_0^2 = 0.5$ in barotropic (left) and baroclinic (right) mode in high-latitude ocean regime. The spectra for the resolved modes $0 < |\mathbf{k}| < 10$ are compared. Black lines with circles show the perturbed model responses in barotropic energy ($\overline{|p_{\psi,k}|^2}$), baroclinic energy ($\overline{|p_{\tau,k}|^2}$), and heat flux ($ik_x\overline{\psi_k^*\tau_k}$). The dashed black lines are the unperturbed statistics. And the reduced order model predictions are in red lines. The last row shows the model prediction from the energy equation in red lines and the energy in the resolved subspace in blue lines. For comparison, the unperturbed and perturbed total energy from the true system are shown in dashed black lines.

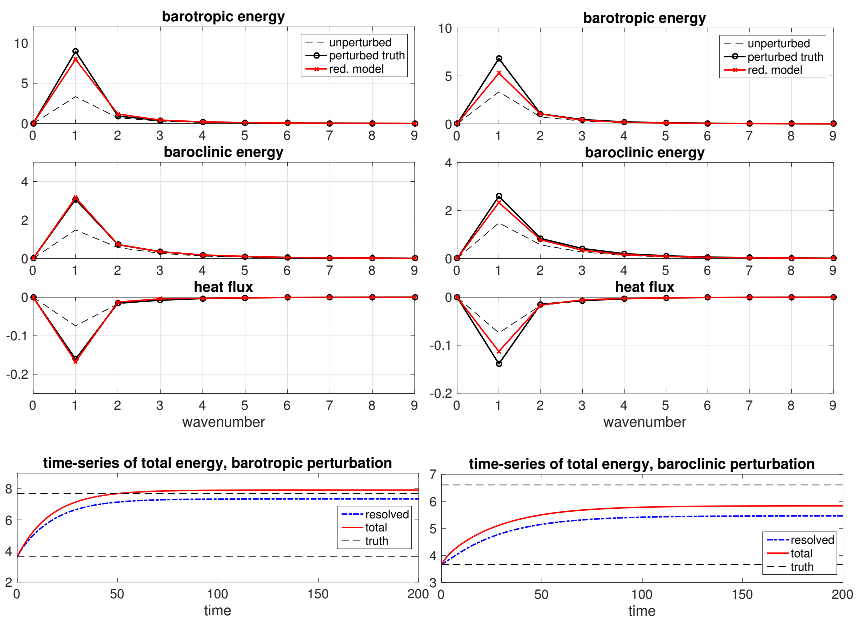

(a) barotropic perturbation (b) baroclinic perturbation

FIG. 12. Reduced-order model predictions to stochastic perturbations with amplitude $\delta\sigma_0^2 = 0.5$ in barotropic (left) and baroclinic (right) mode in high-latitude atmosphere regime. The spectra for the resolved modes $0 < |\mathbf{k}| < 10$ are compared. The last row shows the model prediction from the energy equation in red lines and the energy in the resolved subspace in blue lines. For comparison, the unperturbed and perturbed total energy from the true system are shown in dashed black lines.

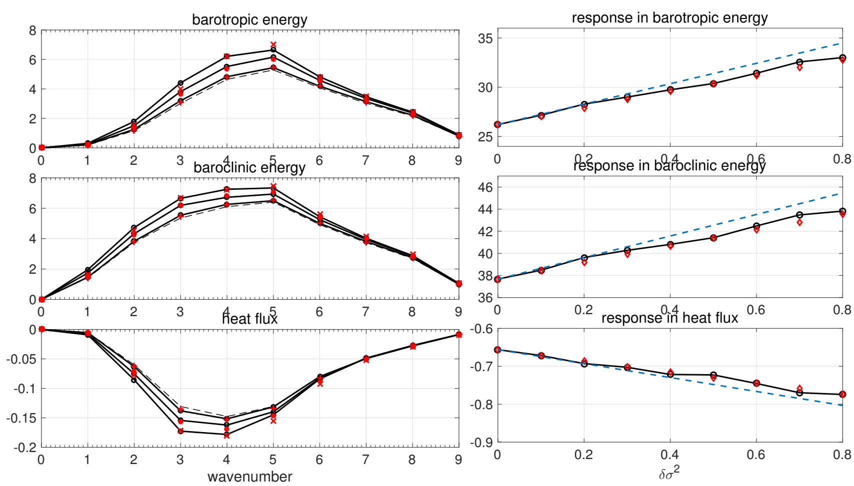

(a) response in spectra (b) total responses

FIG. 13. Imperfect model predictions to responses with changing perturbation amplitudes $\delta\sigma_0^2$ in the high-latitude ocean regime (with barotropic perturbation). In the first part on the left the predicted spectra with three different perturbation amplitudes, $\delta\sigma_0^2 = 0.1, 0.5, 0.8$, are shown. On the right the responses in total energy and heat flux with changing amplitudes $\delta\sigma_0^2 \in [0, 0.8]$ are plotted. For clarification in display, we plot reduced model predictions in red markers and the truth in black lines.

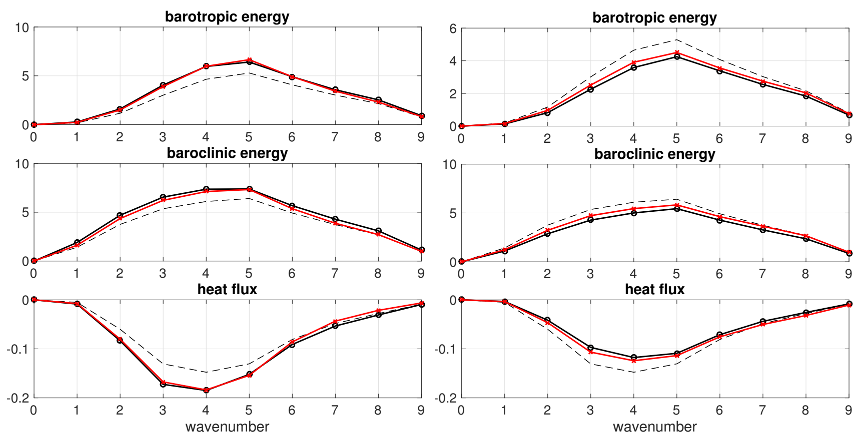

(a) $U = 1.05$ (b) $U = 0.95$

FIG. 14. Reduced-order model predictions to mean shear flow perturbations $\delta U = \pm 0.05$ (that is, 5% of the original value U_0) in the ocean regime. The spectra for the resolved modes $0 < |\mathbf{k}| < 10$ are compared. Black lines with circles show the perturbed model responses in the normalized barotropic energy, baroclinic energy, and heat flux. The dashed black lines are the unperturbed statistics. And the reduced order model predictions are in red lines.

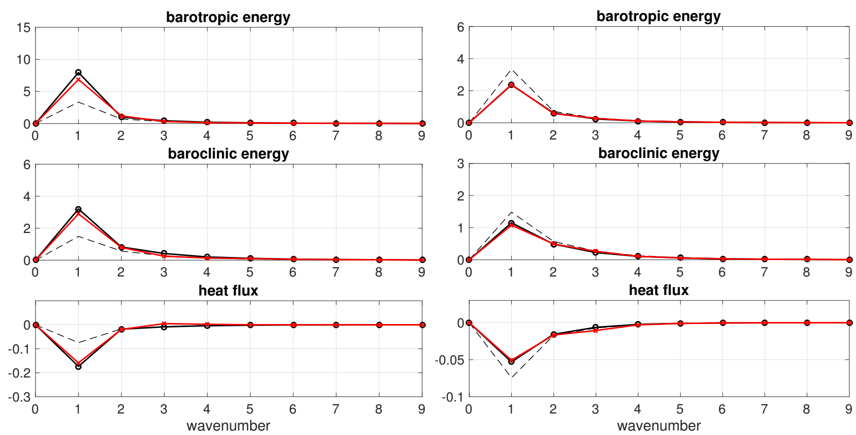

(a) $U = 0.22$ (b) $U = 0.19$

FIG. 15. Reduced-order model predictions to mean shear flow perturbations $\delta U = 0.02, -0.01$ (that is, 5%-10% of the original value U_0) in the atmosphere regime. The spectra for the resolved modes $0 < |\mathbf{k}| < 10$ are compared. Black lines with circles show the perturbed model responses in barotropic energy, baroclinic energy, and heat flux. The dashed black lines are the unperturbed statistics. And the reduced order model predictions are in red lines.

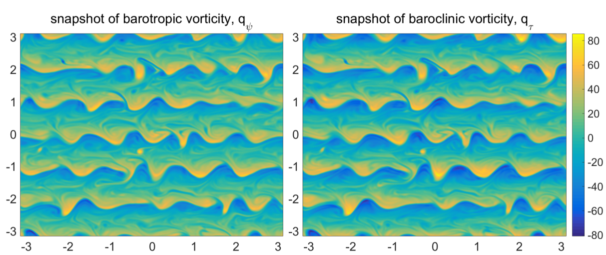

(a) ocean regime

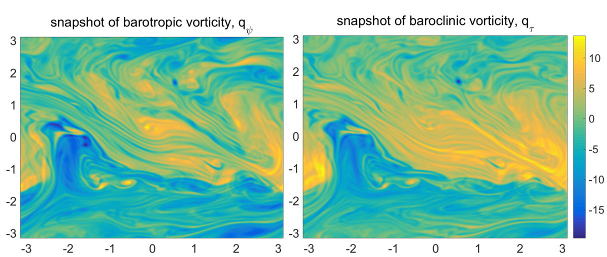

(b) atmosphere regime

FIG. 16. Snapshots of the unperturbed system in low/mid-latitude ocean (upper) and atmosphere (lower) regime. The barotropic and baroclinic vorticity in steady state are plotted. Steady zonal jets can be observed in both regimes.

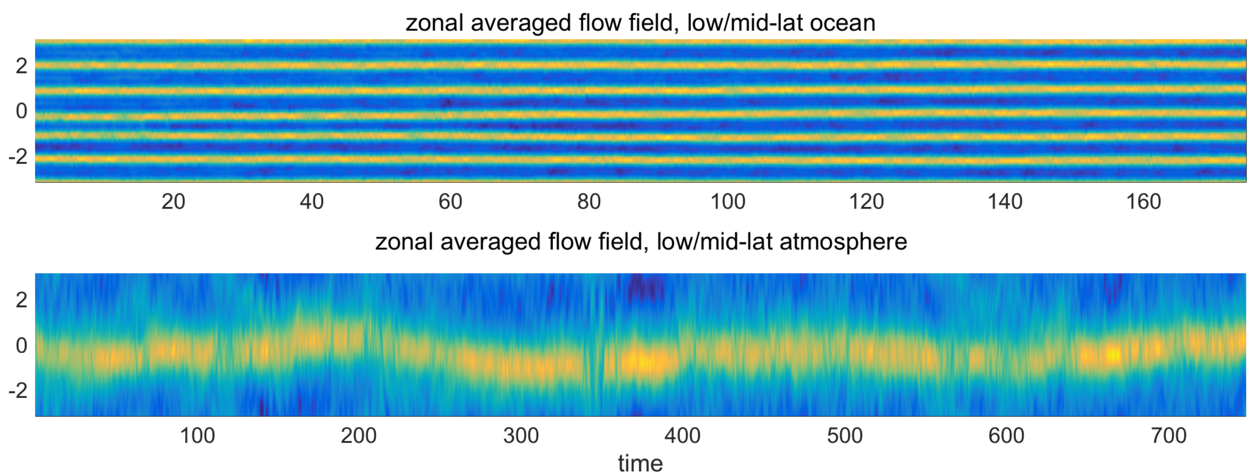

FIG. 17. Time-series of zonal mean flow in low/mid-latitude regime.

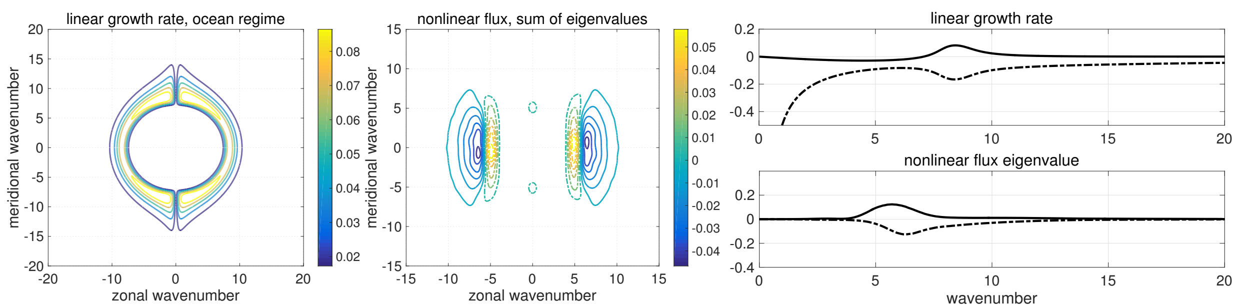

(a) mid/low-latitude ocean regime

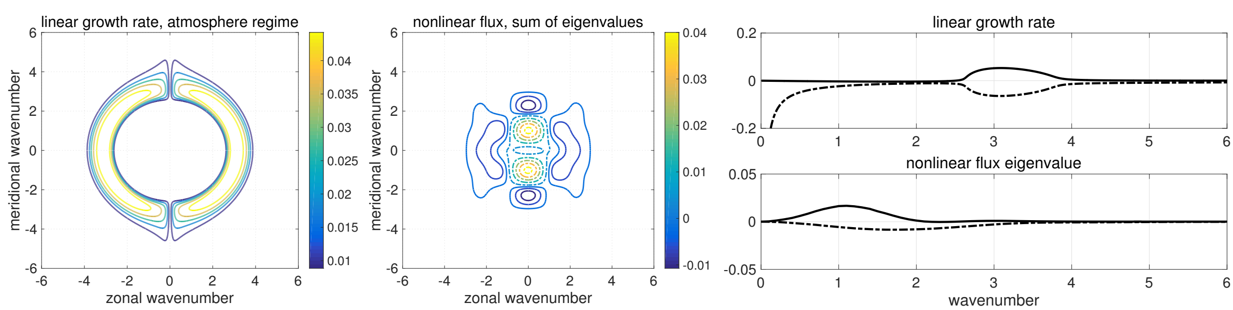

(b) mid/low-latitude atmosphere regime

FIG. 18. Stability from linear analysis and nonlinear flux in ocean (upper) and atmosphere (lower) regime using parameters in Table 2. The growth rate from linear analysis including Ekman damping, and the eigenvalues of the nonlinear flux trQ_F in each wavenumber are displayed in the two-dimensional domain. The last column shows the radial averaged growth rate and eigenvalues in positive and negative components.

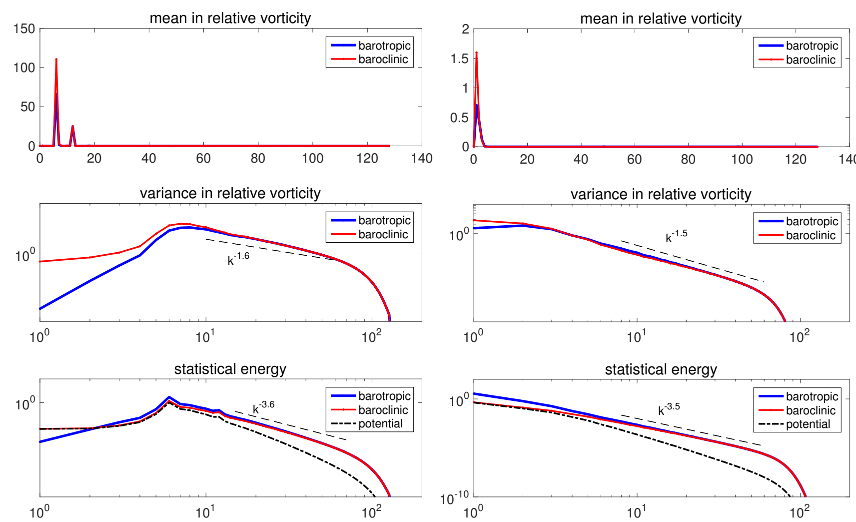

(a) ocean regime (b) atmosphere regime

FIG. 19. Time-averaged statistics (in radial average) in mean and second-order moments in low/mid-latitude regime. The first row compares the statistical mean states. The following two rows show the variances, and statistical energy, in barotropic and baroclinic modes, as well as the potential energy.

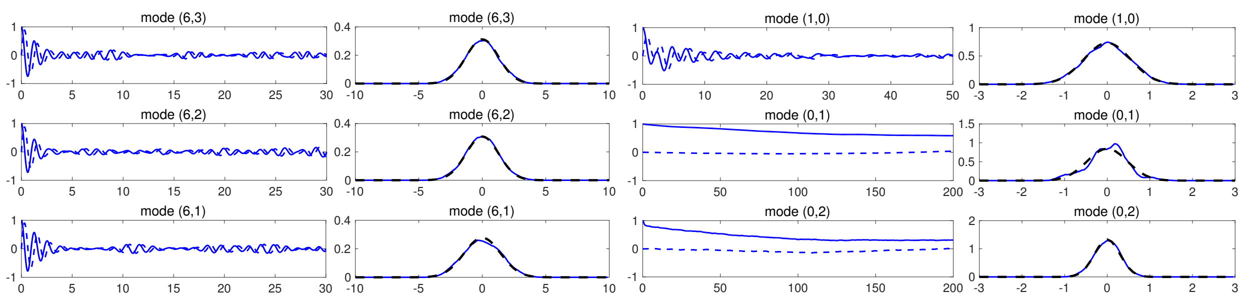

(a) ocean (b) atmosphere

FIG. 20. Autocorrelation functions and the probability distribution functions in low/mid-latitude ocean and atmosphere regime. The first three most energetic baroclinic modes are displayed. In the autocorrelations, the solid lines show the real part while the dashed lines are the imaginary part of the functions. In the PDFs, the corresponding Gaussian distributions with the same variance are also plotted in dashed black lines.

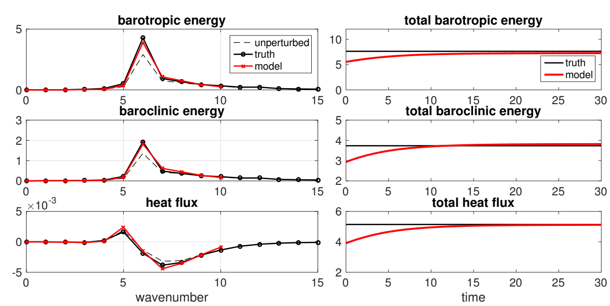

(a) spectra for the energy and heat flux (b) time-series for total responses

FIG. 21. Model responses in low/mid-latitude ocean regime with random forcing perturbation $\sigma_0^2 = 0.2$ (while no stochastic forcing for the unperturbed case). The left panel shows the spectra for the barotropic and baroclinic energy as well as the heat flux. Only first 10 modes are resolved in the reduced-order method. The right panel is the time-series of the (resolved) total energy and heat flux. The truth is shown in black lines.

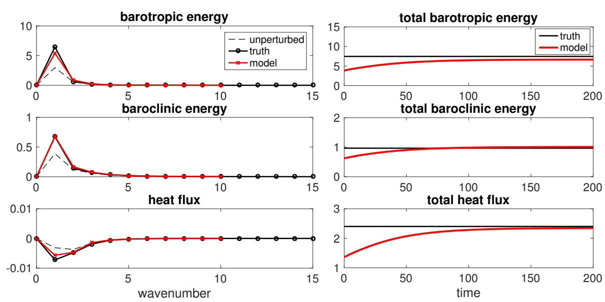

(a) spectra for the energy and heat flux (b) time-series for total responses

FIG. 22. Model responses in low/mid-latitude atmosphere regime with random forcing perturbation $\sigma_0^2 = 0.4$ (while stochastic forcing $\sigma_0^2 = 0.2$ for the unperturbed case). The first mode $\mathbf{k} = (0,1)$ has a large mean state representing the zonal mean flow. The left panel shows the spectra for the barotropic and baroclinic energy as well as the heat flux. Only first 10 modes are resolved in the reduced-order method. The right panel is the time-series of the (resolved) total energy and heat flux. The truth is shown in dashed black lines.